

THE OFFICIAL MAGAZINE OF THE OCEANOGRAPHY SOCIETY

Oceanography

EARLY ONLINE RELEASE

Posted September 15, 2018

CITATION

Desiage, P.-A., J.-C. Montero-Serrano, G. St-Onge, A.C. Crespi-Abril, E. Giarratano, M.N. Gil, and M.J. Haller. 2018. Quantifying sources and transport pathways of surface sediments in the Gulf of San Jorge, central Patagonia (Argentina). *Oceanography* 31(4), <https://doi.org/10.5670/oceanog.2018.401>.

DOI

<https://doi.org/10.5670/oceanog.2018.401>

PERMISSIONS

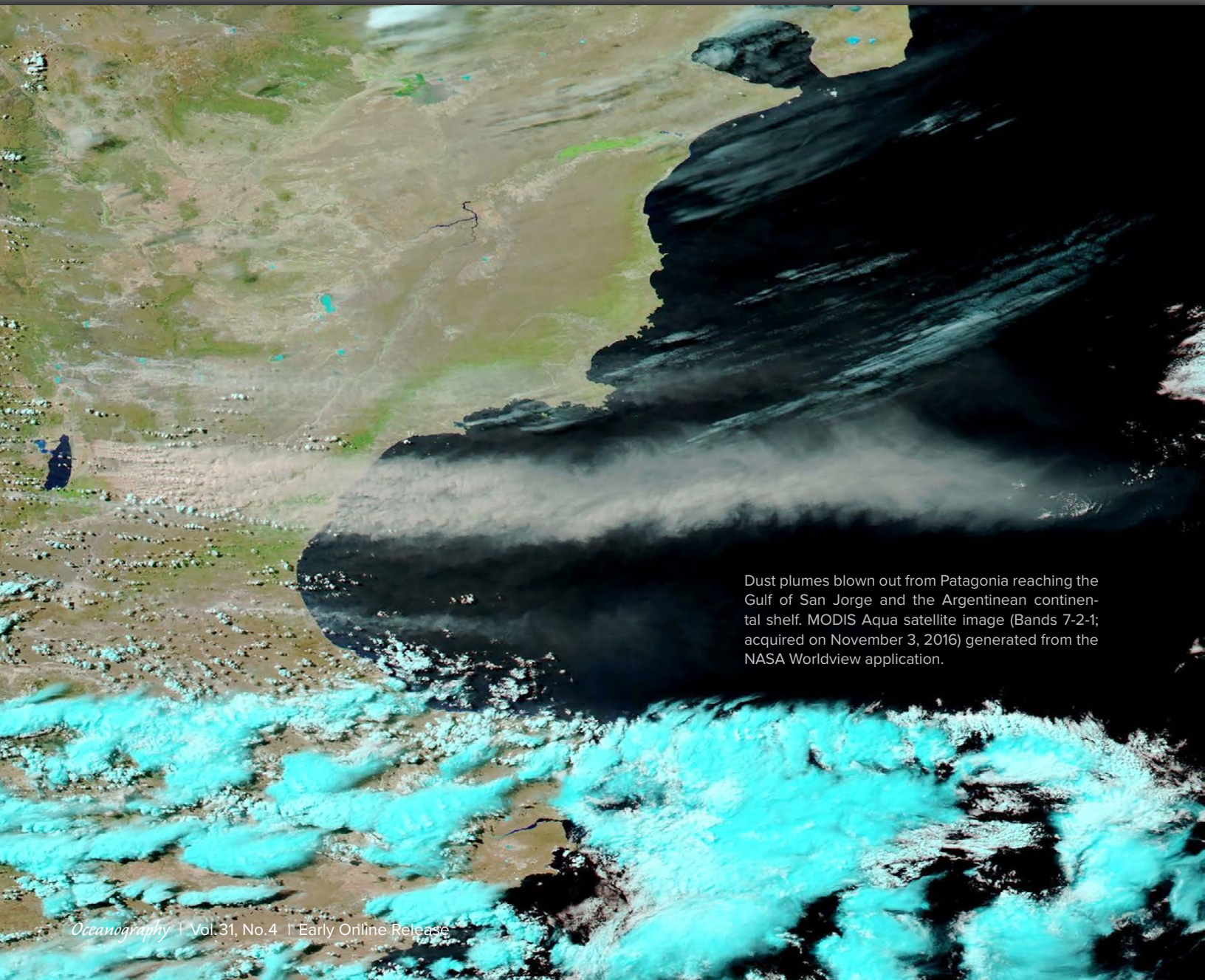
Oceanography (ISSN 1042-8275) is published by The Oceanography Society, 1 Research Court, Suite 450, Rockville, MD 20850 USA. ©2018 The Oceanography Society, Inc. Permission is granted for individuals to read, download, copy, distribute, print, search, and link to the full texts of *Oceanography* articles. Figures, tables, and short quotes from the magazine may be republished in scientific books and journals, on websites, and in PhD dissertations at no charge, but the materials must be cited appropriately (e.g., authors, *Oceanography*, volume number, issue number, page number[s], figure number[s], and DOI for the article).

Republication, systemic reproduction, or collective redistribution of any material in *Oceanography* is permitted only with the approval of The Oceanography Society. Please contact Jennifer Ramarui at info@tos.org.

Permission is granted to authors to post their final pdfs, provided by *Oceanography*, on their personal or institutional websites, to deposit those files in their institutional archives, and to share the pdfs on open-access research sharing sites such as ResearchGate and Academia.edu.

QUANTIFYING SOURCES AND TRANSPORT PATHWAYS OF SURFACE SEDIMENTS IN THE GULF OF SAN JORGE, CENTRAL PATAGONIA (ARGENTINA)

By Pierre-Arnaud Desiagne, Jean-Carlos Montero-Serrano, Guillaume St-Onge,
Augusto César Crespi-Abril, Erica Giarratano, Mónica Noemí Gil, and Miguel J. Haller



Dust plumes blown out from Patagonia reaching the Gulf of San Jorge and the Argentinean continental shelf. MODIS Aqua satellite image (Bands 7-2-1; acquired on November 3, 2016) generated from the NASA Worldview application.

ABSTRACT. The Gulf of San Jorge (GSJ) is a semicircular basin, approximately 160 km long and 250 km wide, located in the central part of Patagonia between 45°S and 47°S, lacking any present-day major perennial tributaries. The grain size and bulk and clay mineralogical compositions as well as major and minor elements of 75 surface sediment samples from the GSJ and the adjacent continental shelf were investigated to define the spatial distribution, transport pathways, and potential sources of terrigenous material. To better constrain the origins of GSJ sediments, analyses were also performed on 14 terrestrial, riverine, and marine samples from potential source areas around the gulf and Patagonia. The mineral assemblage of surface sediments in the gulf, dominated by plagioclase, quartz, and clays, is a function of the primary continental volcanic geology of Patagonia. The significant concentration of volcanoclastic particles indicated by mineralogical signatures and scanning electron microscope images of sediments suggests a substantial contribution from rhyolitic volcanism to the modern sedimentation in the gulf. High amounts of smectite are carried into the GSJ by dust transport, whereas inputs of chlorite and illite seem to be associated with continental shelf current transport from southern Patagonia. Finally, our results suggest that 50% of the surface sediment in the GSJ is derived from external/oceanic inputs, 40% from inner gulf shores (i.e., erosion and runoff), and 10% from dust (i.e., aeolian transport).

INTRODUCTION

Key oceanographic processes, such as biogeochemical cycles, primary production, and sediment transfer to deeper waters, occur on continental shelves, which lie between terrestrial/coastal and oceanic domains. Because they are partially landlocked and partially open to the ocean, gulfs provide suitable small-scale analogs for the mechanisms occurring on the continental shelf. Furthermore, large coastal embayments such as gulfs are often sensitive marine environments affected by human activities (e.g., fisheries and/or urban development). Located in the central part of the Argentine continental shelf (ACS), the Gulf of San Jorge (hereafter referred to as GSJ; [Figure 1](#)) provides a perfect example of both economical-industrial development and environmental preservation. Indeed, numerous foraging and reproduction areas for marine birds and mammals coexist in the GSJ with commercial shrimp and hake fisheries, as well as terrestrial oil production.

In this strategic environmental and oceanographic context, numerous studies focusing on the grain size and mineralogical and geochemical composition of the detrital sediments over gulfs and continental shelves have been performed to determine their sources and depositional conditions and to identify their transport

pathways as well as regional hydrodynamic patterns (e.g., [Preda and Cox, 2005](#); [Spagnoli et al., 2008](#); [Saukel et al., 2010](#)). A growing number of studies also work with bulk mineralogy, clay mineralogy, and elemental geochemistry to characterize modern sedimentary processes and to determine the provenance of terrigenous sediments (e.g., [Andrews and Vogt, 2014](#); [Gamboa et al., 2017](#)).

On the Argentinean continental shelf and margin, the physical and chemical properties of surface and subsurface sediments have been characterized via bulk and clay mineralogy and elemental and isotopic geochemistry (e.g., [Petschick et al., 1996](#); [de Mahiques et al., 2008](#)). All these results contributed to investigations of the composition and provenance of terrigenous inputs. Additionally, the chemical signatures of rivers, aeolian dust, and topsoil samples have been analyzed to estimate the potential riverborne and windborne inputs to the Patagonian littoral ([Gaiero et al., 2004, 2007](#)). However, most of the coastal studies, as well as the sampling campaigns, have been conducted in the northern region of the ACS and especially in the Río de La Plata estuary at ~35°S (e.g., [Nagai et al., 2014](#)). This focus leads to a disproportionate amount of information available for the north compared to the other coastal and inner

shelf areas of Argentina.

In this study, we present the first multiproxy analysis based on grain-size distribution, bulk and clay mineralogy, and elemental geochemistry (major and trace elements) of surface sediments from the GSJ. The main objectives of this study were to (1) characterize the spatial distribution of the surface sediments, and (2) define the different sources and transport processes of detrital sediment in the GSJ. Samples from potential source areas (such as beaches, tablelands, dry-bed lakes, river mouths, and oceanic environments) were also analyzed to document the relative differences between the sediment composition in the potential source areas and sediment samples from the GSJ.

STUDY AREA

Physical Setting

The Patagonian continental shelf represents the southern part of the ACS and is delimited by the Patagonian coast from Cape Horn (55°S) nearly to the Colorado River (39°S). The hydrodynamics of the region consists of a northward (NNE) flow of sub-Antarctic cold water (i.e., Patagonian Current; [Figure 1a](#)) conveyed onto the shelf through the Cape Horn Current and the Malvinas Current along the continental slope ([Palma et al., 2008](#), and references therein).

The Atlantic coast of Patagonia is therefore characterized by a dry climate (from 200 mm yr⁻¹ to 400 mm yr⁻¹ rainfall; [Coronato et al., 2008](#)). The strongest winds are concentrated between 49°S and 53°S in the heart of the southern westerly winds belt ([Kilian and Lamy, 2012](#)). The surface hydrology consists of eight main watercourses, mostly perennial, draining toward the east from Andean headwaters to the Atlantic. Except for the Negro River in the north and the Santa Cruz River in the south, the other major watercourses have relatively limited discharge ([Figure 1a](#); [Kokot, 2004](#)).

The GSJ is a semicircular basin, approximately 160 km long and 250 km wide, located in the central part of Patagonia between 45°S (Cape Dos Bahías) and

47°S (Cape Tres Puntas; Figure 1b,e), an encroachment of the South Atlantic Ocean in the heart of southern South America. The bathymetry of the basin rapidly decreases to reach the 90 m isobath, which defines a large flat central region that covers most of the surface of the gulf and corresponds to the Patagonian outer shelf (Violante et al., 2014). The hydrodynamic and water mass origins in the gulf are related to the northward circulation on the shelf (Figure 1a; Palma et al., 2008), but the GSJ is also located at the limit of the influence of the Magellan Strait discharge flowing along the coast and entering the gulf in the southeastern sector at Cape Tres Puntas (Fernández et al., 2005).

From geological and geographical points of view, most of the GSJ forms the eastern part of the hydrocarbon-producing San Jorge Gulf Basin that is surrounded by the North Patagonian Massif to the north, the Deseado Massif

to the south, and the Andes to the west (Sylwan, 2001). The presence of these two massifs is expressed in the GSJ area by Jurassic silicic volcanic rock outcrops, predominantly rhyolitic, from the Chon Aike province (Figure 1a; Pankhurst et al., 1998). The main outcrop of silicic rocks, dominated by rhyolites and ignimbrites, is located in the northeastern part of the gulf close to Cape Dos Bahías and covers the entire sector of the Patagonia Austral Marine Park (hereafter referred to as marine park; Figure 1a,b; Pankhurst et al., 1998). The tablelands of the San Jorge Gulf Basin are mainly overlain by Eocene-Miocene sedimentary rocks of the Sarmiento and Patagonia Formations (Cuitiño et al., 2015), as well as Quaternary fluvio-glacial deposits (e.g., “Rodados Patagónicos”; Martínez and Kutschker, 2011). The tablelands reach the coast as cliffs or beach-ridge systems, and are generally composed of gravel and/or sand (Isla et al., 2002).

Sedimentation

The main suppliers of terrigenous materials to the Patagonian littoral are coastal erosion, rivers, and aeolian transport, as well as transportation and redistribution of sediments from the shelf by the prevailing northward-flowing Patagonian Current. Indeed, according to Pierce and Siegel (1979) and Gaiero et al. (2003), the estimated contributions of coastal erosion, dust transport, and rivers to the terrigenous sedimentary supply transferred offshore are, respectively, 56%, 41%, and 3% (Violante et al., 2014). The weak proportion of sedimentary inputs to the continental shelf by the Patagonian rivers is explained by their present low flows and the low particulate loads in their downstream sectors (Gaiero et al., 2003; Kokot, 2004). The large aeolian contribution results from a combination of strong westerly winds over the regional geomorphology and the arid climate, which stimulates the resuspension and

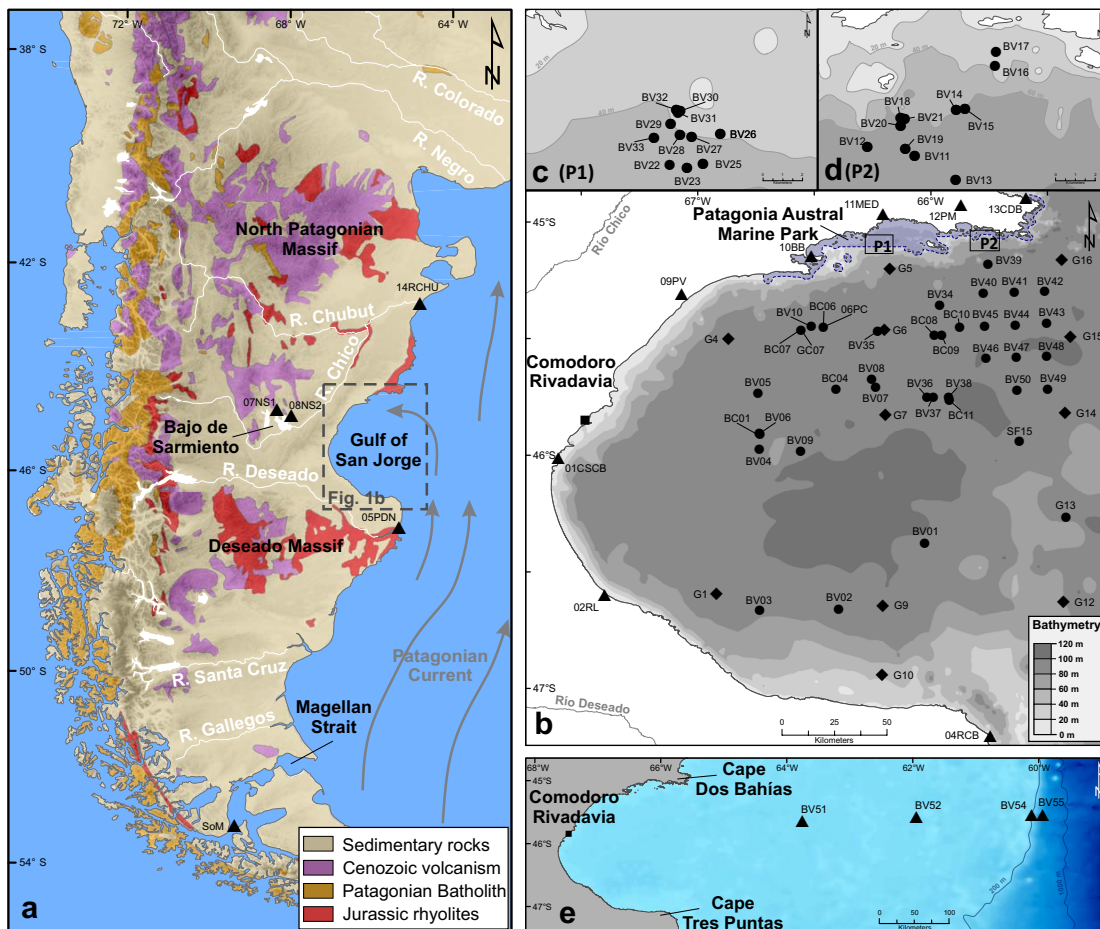


FIGURE 1. Maps of the study area with sample locations. The dots indicate surface sediment samples in the Gulf of San Jorge (GSJ), the diamonds denote sites with surface sediment samples as well as water column filters, and the triangles illustrate samples from potential source areas. (a) Map of Patagonia showing the main hydrodynamic circulation on the Patagonian continental shelf (gray arrows; Palma et al., 2008), simplified surface geology, and main geographic features mentioned in the text. (b–d) Bathymetric maps of the Gulf of San Jorge and marine park areas. (e) Bathymetric map of the GSJ with adjacent continental margin.

transport of surficial terrestrial sediments from Patagonian tablelands to the shelf (Crespi-Abril et al., 2018).

The GSJ does not have any present-day major and perennial tributaries likely to strongly affect the sedimentation. Furthermore, the gulf is located in the heart of several hundred kilometers of littoral without major rivers, except for the relatively low flow of the Deseado River ($5 \text{ m}^3 \text{ s}^{-1}$; Kokot, 2004), which reaches the ocean a few dozen kilometers south of the GSJ (Figure 1a). However, there are aeolian inputs to the Gulf area (Isla et al., 2002; Crespi-Abril et al., 2016), as the basin is located on the outskirts of major dust sources (Prospero et al., 2002).

MATERIAL AND METHODS

Seventy-five marine surface samples were collected in the GSJ, as well as on the continental shelf. The sampling was performed using a Van Veen grab sampler (65 samples), a box corer (8 samples), a gravity corer (1 sample), and a piston corer (1 sample) wherein the uppermost 1 cm of sediment was recovered to collect only the sediment-water interface (Figures 1b–e). These core-top sediments were found to represent modern

time or at least the last decade/century when the topmost centimeters were missing. All marine samples were recovered on board R/V *Coriolis II* from January 29 to March 4, 2014 (Leg 1: MARES and Leg 2: MARGES), as part of the PROMESSE (PROgrama Multidisciplinario para el Estudio del ecosistema y la geología marina del golfo San Jorge y las costas de las provincias de Chubut y Santa Cruz) project. Bulk and clay mineralogy and elemental geochemistry were analyzed for all samples, whereas grain size analysis was performed on only 57 samples due to the low quantity of sediments available for the Leg 1 stations. The 63–300 μm and <63 μm sediment fractions of three selected samples (BV01, BV06, and BC11) were also examined using a scanning electron microscope (SEM) to determine the abundance and the geochemical character of volcanoclastic particles (e.g., glass shards) in the marine sediments. In addition, 13 terrestrial and riverine samples as well as a marine surface sediment sample (0–2 cm sediment depth) from the Magellan Strait were analyzed for their mineralogical and elemental geochemistry signatures (see details in the supporting information; Figure 1a,b).

To document the chemical composition and geochemical classification of suspended sediments in the water column, 22 seawater samples from 11 stations were recovered in the GSJ during the MARES cruise (Figure 1b). For each station, seawater samples were collected using Niskin bottles fixed on a CTD rosette both at the sea surface (2 m depth) and close to the seafloor. Between 0.5 L and 1.5 L of seawater, depending on particle load, was filtered onto glass-fiber GF/F filters. The filters were stored frozen at -20°C until they could be analyzed.

The source samples and detailed methodology used for the analyses of grain size, SEM, bulk and clay mineralogy, and elemental geochemistry, as well as the statistical approach are presented in the online supplementary material.

RESULTS

Grain-Size Distribution

In the GSJ, the analyzed sediments are mostly fine to very fine silts, as well as very fine sands with a mean grain size (Φ scale) ranging from 8.01 (very fine silt) to 3.73 (very fine sand; Figure 2b, Figure S1a, and Table S1). Coarser sediments are dominant for the northern

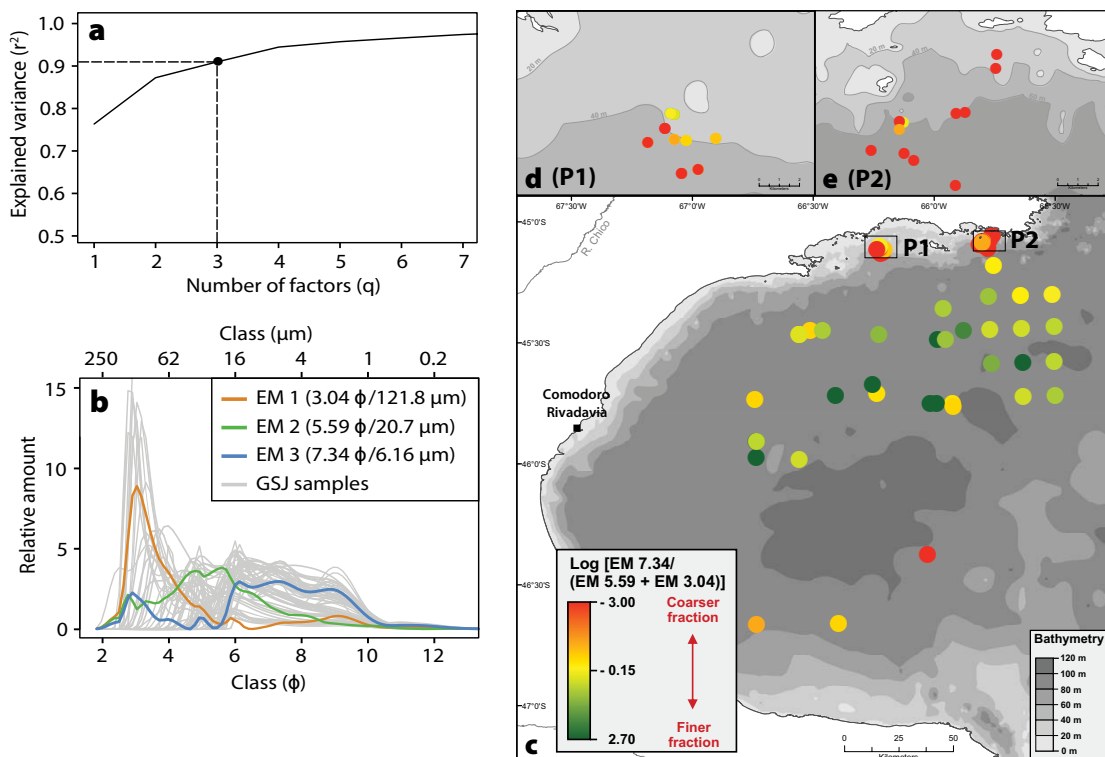


FIGURE 2. End-member modeling analysis (EMMA) performed on the detrital fraction of the grain-size distribution in the GSJ. (a) The grain-size distribution of the first three end members accounts for more than 91% of the variance. (b) Three representative unmixed grain-size distributions produced from EMMA based on the grain-size distributions of the GSJ samples (gray lines). (c–e) Log[EM3/(EM2+EM1)] end-member ratios in the GSJ and marine park areas, respectively.

coastal sample patches (marine park area; Figure S1b,c), especially close to the Cape Dos Bahías area (P2; Figure S1c). Fine silts prevail in the north-central area of the GSJ, with a finer fraction in the inner part of the gulf (Figure S1a). The mean sediment grain size measured in the GSJ for this study coincides with results obtained by Fernández et al. (2003). Furthermore, end-member modeling analysis (EMMA) provides a model with three end members (EM) that explain 91% of the variance in the grain size data set (Figure 2a). Based on the grain size distributions of the three end members (Figure 2b), EM1 represents a well-sorted distribution associated with the very fine sand fraction (mean $\sim 3.04 \Phi$), EM2 shows a well-sorted distribution associated with the coarse and medium silt fractions (mean $\sim 5.29 \Phi$), and EM3 represents a well-sorted distribution with main peaks corresponding to the finer grain fractions (i.e., fine silt to clay; mean $\sim 7.34 \Phi$). EM1 and EM2 characterize all the samples from the park area

(P1 and P2), as well as the three samples from the southern part of the gulf, and EM3 represents most of the samples from the north-central area (Table S1). Maps of the $\log[EM3/(EM2+EM1)]$ end-member ratios are used to illustrate the spatial variations of the relative proportion between very fine silt and coarse silt to identify the mechanism of transport/sources of particles in the GSJ (Figure 2c–e).

Bulk Mineralogy

The most abundant minerals in the GSJ bulk sediments, identified according to the quantitative X-ray diffraction (qXRD) method developed by Eberl (2003), are quartz (14%–51%), plagioclase (15%–49%), clays (2%–41%), amorphous silica (4.5%–35.5%), and K-feldspar (2%–12%). The bulk mineralogical compositions of sediments also indicate smaller proportions of pyroxene ($<2.7\%$), amphibole ($<1.5\%$), and Fe-oxides ($<0.9\%$; Table S2). Amorphous silica can mostly be identified as volcanic

rhyolitic tephra based on the Icelandic tephra sample (Hekla-4), which is used as a mineral standard in RockJock v11 (Andrews et al., 2013). Indeed, in the XRD scans centered between 19° and 31° two-theta, the samples containing higher proportions of amorphous silica ($>10\%$; e.g., BV01; Figure S3a) present patterns similar to the standard of rhyolitic tephra (Hekla-4). Furthermore, SEM imaging of the sediments in the 63–300 μm fraction from the BV01, BV06, and BC11 sites attests to the appreciable amounts of volcanoclastic particles, which are mainly represented by highly vesicular glass shards and slightly vesicular glass shards with blocky to curvilinear shapes (Figure S3b,c). SEM images also show the near absence of diatom frustules, considered to be the other potential source of amorphous silica. The geochemical data in $\text{K}_2\text{O}-\text{SiO}_2$ of glass shards in the surface sediments confirm the rhyolitic composition of volcanoclastic particles in surface sediments (Figure S3d). The bulk mineralogy is presented in a ternary diagram showing the three most abundant minerals (quartz, plagioclase, and clays) in the GSJ samples (Figure 3). The ternary diagram also includes results from bulk mineralogy analyses of marine and terrestrial sediments from the Patagonian continental shelf, Strait of Magellan, and San Jorge Gulf Basin, all representing potential source areas of sedimentary inputs to the GSJ (Figure 3). The ternary diagram reveals that the clay content differs significantly between sediments from marine park areas and those from most of the other parts of the gulf. Indeed, the sites in the marine park areas are characterized by lower concentrations of clays (2%–10.5%) with homogeneous values of quartz and plagioclase (26%–42% and 34%–49%, respectively) in contrast to the clay contents in the other parts of the GSJ, which are higher (6%–41%), with scattered values of quartz and plagioclase (14.5%–51% and 16.5%–37%, respectively).

To visualize the main tendencies of mineralogical enrichment in the gulf, spatial distributions of mineralogical

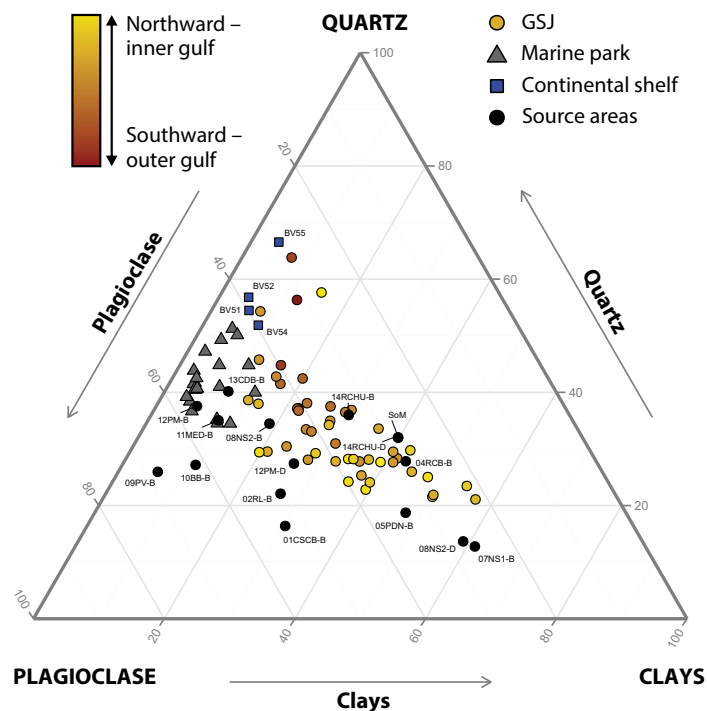


FIGURE 3. Quartz-plagioclase-clays ternary plot illustrating the relative compositions of the main minerals. The samples are illustrated according to their locations in the Gulf of San Jorge; the northward-inner gulf to southward-outer gulf tendency is calculated from absolute latitude and longitude coordinates (excluding the park sites).

balances for major mineral groups (i.e., $b_{\{(Quartz+Feldspars)/Clays\}}$) were conducted (Figure 4a; see statistical details in the online supporting information). The results indicate higher values associated with quartz and feldspar enrichments versus clay enrichment for the marine park areas. The lower values are related to most of the other parts of the GSJ, with the exception of intermediate values for samples located in the northern and southern outer parts of the Gulf (Figure 4a).

To confirm the five-source composition, SedUnMix was run with the five sources against the source area samples previously used to define the source compositions (see details in supplementary material; Table S5). The results indicate a high proportion of sources S1, S2, S4, and S5 to the sediment composition of their respective source samples

(from 65% to 100%; Table S4). The contribution of source S3 to its representative source samples is weaker (from 7% to 47%; Table S4), and proportions are mainly shared with source S5. Spatial distributions for the proportions of inner gulf coastal inputs (S1 + S2), dust transport (S4) and external/oceanic contributions (S3 + S5) to sediment mineralogical composition are presented respectively in Figure 4b–d. Sources S1 and S2 are abundant in the sediment assemblage of the coastal park areas and the northeast-central part of the GSJ (>40% with mean value ~70% close to the park). The proportions of sources S1 and S2 in sample composition are comparatively low for the other sectors of the GSJ (<30%; Figure 4b). The results from Figure 4c indicate that a low to intermediate fraction of the sediment assemblage

is associated with source S4 (<50%), with distribution limited to approximately ten samples in the northwestern and central parts of the GSJ. Nevertheless, this study focuses on the aeolian transport of silt and clay fraction particles using the <63 μm fraction of 08NS2 and the fine dry-bedload sediment from 07NS1 as source samples to generate a dust-related source (S4) in SedUnMix. Thus, we consider only the intermediate- to long-distance aeolian transport. This bias could have led to underestimating the wind-blown “coarse” dust, which is known to be deposited in the region as shown by the creation and displacement of dune fields south of Comodoro Rivadavia (Montes et al., 2015). S3 and S5 combined represent the source with the highest contribution to the sediment composition of the Gulf, excluding the

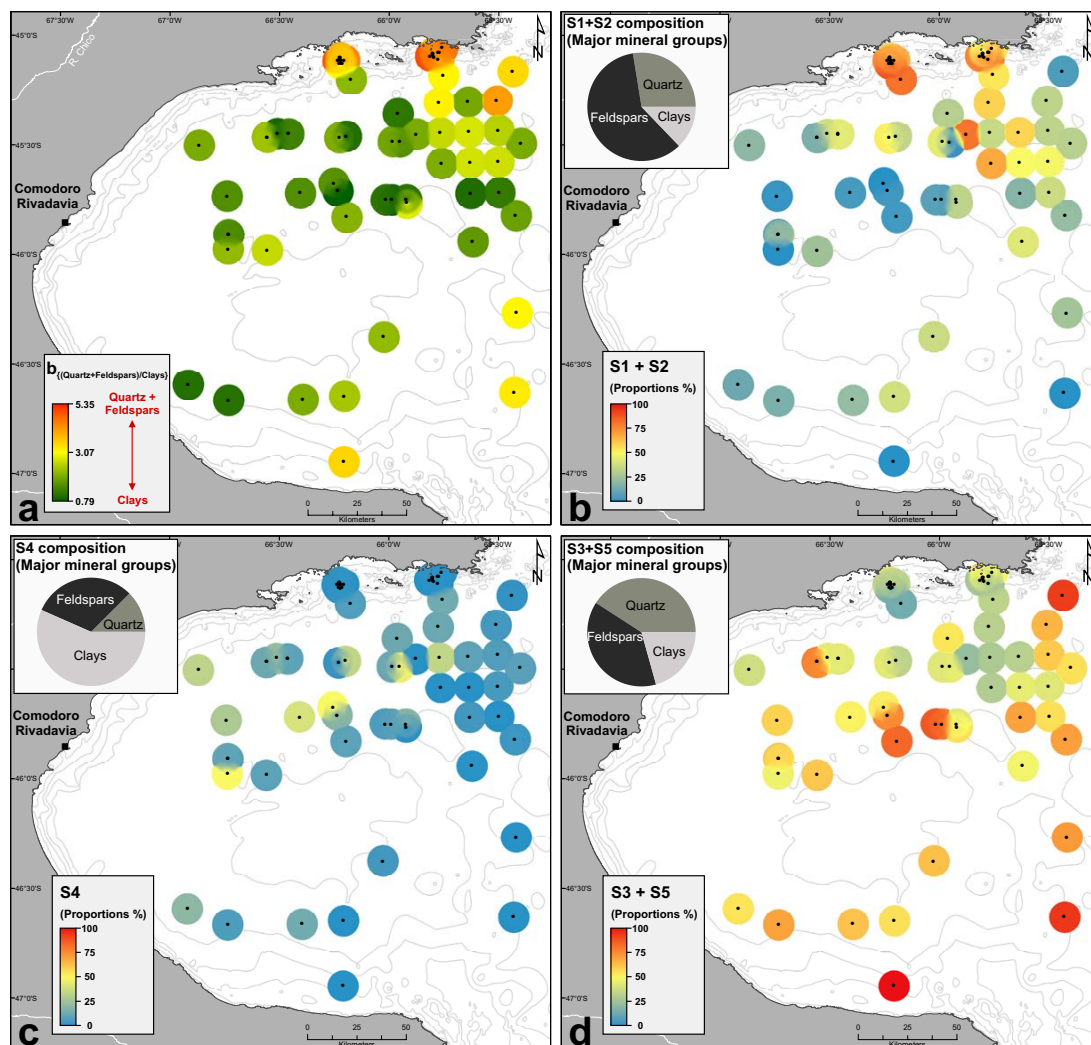


FIGURE 4. (a) Spatial distribution of the elemental balance for major mineral groups (i.e., $b_{\{(Quartz+Feldspars)/Clays\}}$). (b–d) Maps showing relative proportions of inner gulf coastal inputs (S1 + S2; b), dust transport (S4; c) and external/oceanic contributions (S3 + S5; d) to sediment mineralogical composition. The proportions in major mineral groups (quartz, feldspars, and clays) of proposed sources (S1 + S2, S4, and S3 + S5) are presented in pie charts.

coastal park areas, especially in the central sector (from 47% to 86%), in the southwest part (from 50% to 100%), and in the oceanic perimeter of the GSJ (from 56% to 100%; Figure 4d).

Elemental Geochemistry

The major element composition of bulk sediments from the GSJ is characterized by very high proportions of SiO₂, high

contents of Al₂O₃, and lower concentrations of Fe₂O₃, CaO, K₂O, MgO, TiO₂, P₂O₅, and MnO (Table S3). Sr, Zr, and V dominate the minor and trace elements. The sediment samples are plotted in the log(SiO₂/Al₂O₃) versus log(Fe₂O₃/K₂O) classification diagram (Herron, 1988) coupled with the results of the water sample filters (surface and bottom) to compare the geochemical classification and

mineralogical maturity between sediment from the seafloor and the water column (Figure 5c). The seafloor sediments and suspended sediment in the water column are geochemically classified as shale and wacke with no major distinction concerning the dispersion in the diagram of the seabed and suspended sediment samples.

The ternary diagrams Al-Si-Fe and

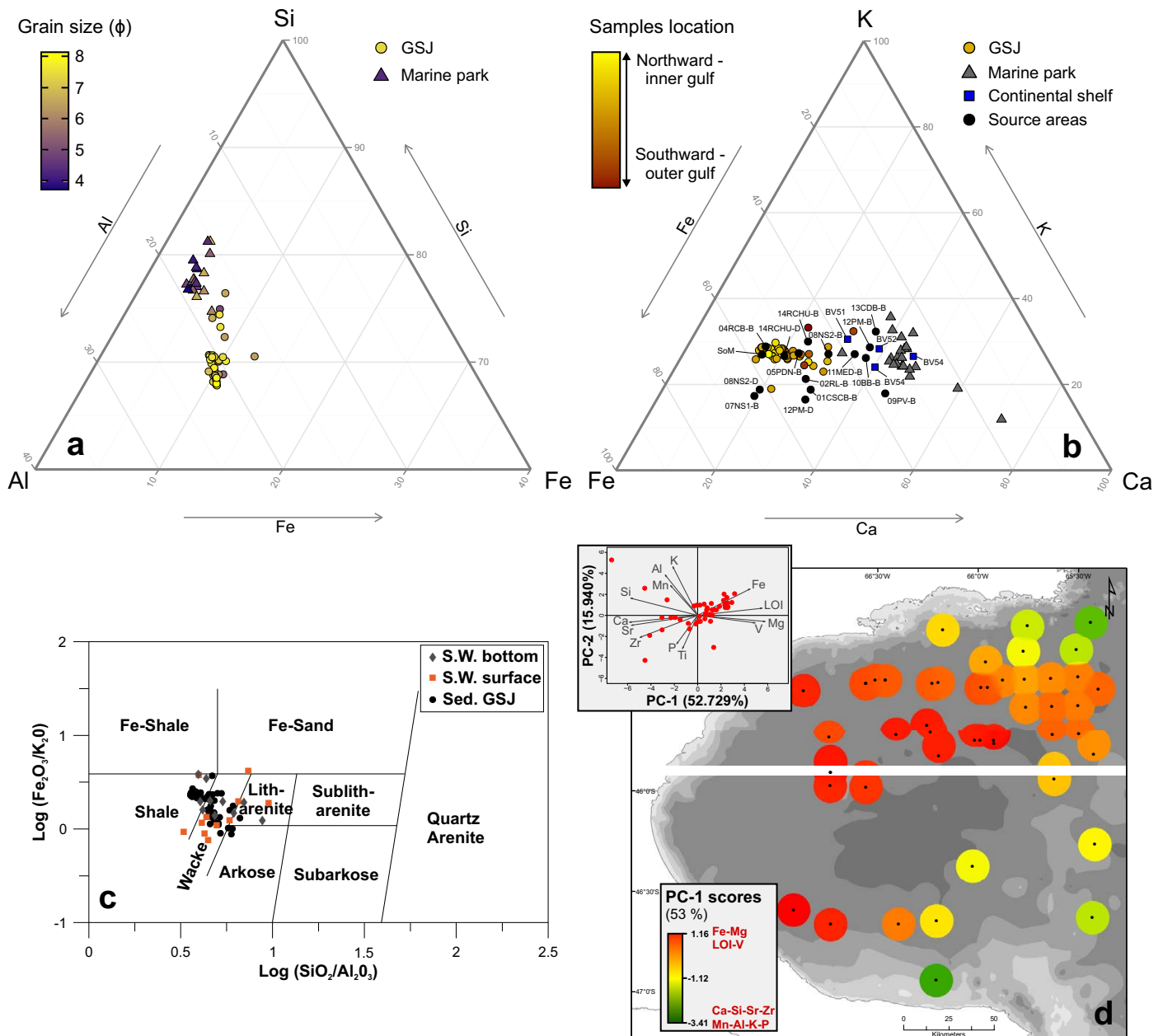


FIGURE 5. (a) Si-Al-Fe abundances of marine park areas and other GSJ samples associated with mean grain size (Φ). (b) K-Fe-Ca distribution of marine park areas and other GSJ samples, plotted together with potential source area samples, as well as surface sediment samples from the Patagonian continental shelf (Table S3). The samples are illustrated according to their location in the gulf; northward-inner gulf to southward-outer gulf tendency calculated from absolute latitude and longitude coordinates (excluding the park sites). (c) Herron (1988) geochemical classification diagram for surface sediment and water column samples of the GSJ. (d) Biplot of the PC-1 versus PC-2 generated from the log-centered transformation of major, minor, and trace elements of GSJ samples, presented with map of PC-1 scores.

Fe-K-Ca (Figure 5a,b; see details in the online supporting information) highlight the clear distinction between coastal park areas and central GSJ samples with higher relative proportions of Si (>74%; Figure 5a) and Ca (>38%; Figure 5b) in the park. The enrichment in Si seems positively correlated with coarser sediments (Figure 5a).

We illustrate the scores from the first two principal components of the log-centered geochemical data (excluding the geochemically distinctive areas of the coastal park) as they account for more than 69% of the total variance (Figure 5d). PC-1 scores account for 53% of the total variance and appear to be positively correlated with Fe-Mg-V-LOI and negatively correlated with Ca-Si-Sr-Zr-Mn-Al-K-P. The spatial distribution of PC-1 elemental geochemical scores indicates that high values dominate the central and southwest parts of the gulf and are associated with enrichment in Fe, Mn, and V in these areas (Figure 5d). These results expose a noticeable tendency similar to that of the bulk mineralogy distribution in the GSJ with higher enrichments in clays in the central and southwest parts of the GSJ (Figure 5a). Limited sectors in

the northeast and southeast parts of the GSJ, close to Capes Dos Bahias and Tres Puntas, present intermediate to low PC-1 scores (Figure 5d).

Clay Mineralogy

The clay mineral assemblage of sediment in the gulf is highly dominated by smectite with a contribution of more than 75% for at least 85% of the samples. In contrast, chlorite, illite, and kaolinite contents are rather low with average contributions close to 8%, 6.5%, and 1.5%, respectively (Table S2). The relative abundances of kaolinite, smectite, and coupled illite plus chlorite (I+C) of the GSJ samples, as well as marine and terrestrial samples associated with potential source areas for sedimentary inputs in the GSJ, are plotted in a ternary diagram (Figure 6a,b). The results confirm the high proportions of smectite in GSJ sediment, especially in the coastal park areas (Figure 6b). The spatial distribution of the $\log[\text{smectite}/(\text{illite}+\text{chlorite})]$ ratios shows that the higher values occur in the southern part and on the oceanic perimeter of the gulf, excluding the northeast sector, suggesting enrichment in I+C in these regions (Figure 6c).

SEDIMENT DISTRIBUTION, POTENTIAL SOURCE AREAS, AND TRANSPORT PATHWAYS

In the GSJ, grain size analysis and distribution are used to highlight two clearly distinct sedimentary environments. The dominance of coarser sediments (i.e., very fine sand) in the northern part of the gulf in the coastal marine park areas reflects moderate- to high-energy environments (erosive environments; Fernández et al., 2003). These sediments are mainly associated with EM1, especially the sediments close to Cape Dos Bahías, and to a lesser extent with EM2. Due to the absence of riverine inputs in the GSJ, we suggest that the well-sorted fine sand EM1 can be associated with sediments derived from local erosion (i.e., beach and cliff erosion; Isla et al., 2002), and the well-sorted coarse to medium silt EM2 with wind-blown “coarse” dust from nearby sources such as dune fields on the outskirts of the GSJ (Montes et al., 2015). The second distinct sedimentary environment is observed in the central part of the gulf with fine to very fine silts corresponding to a depositional environment with low energy (Fernández et al., 2003). The sediments in this area are almost exclusively

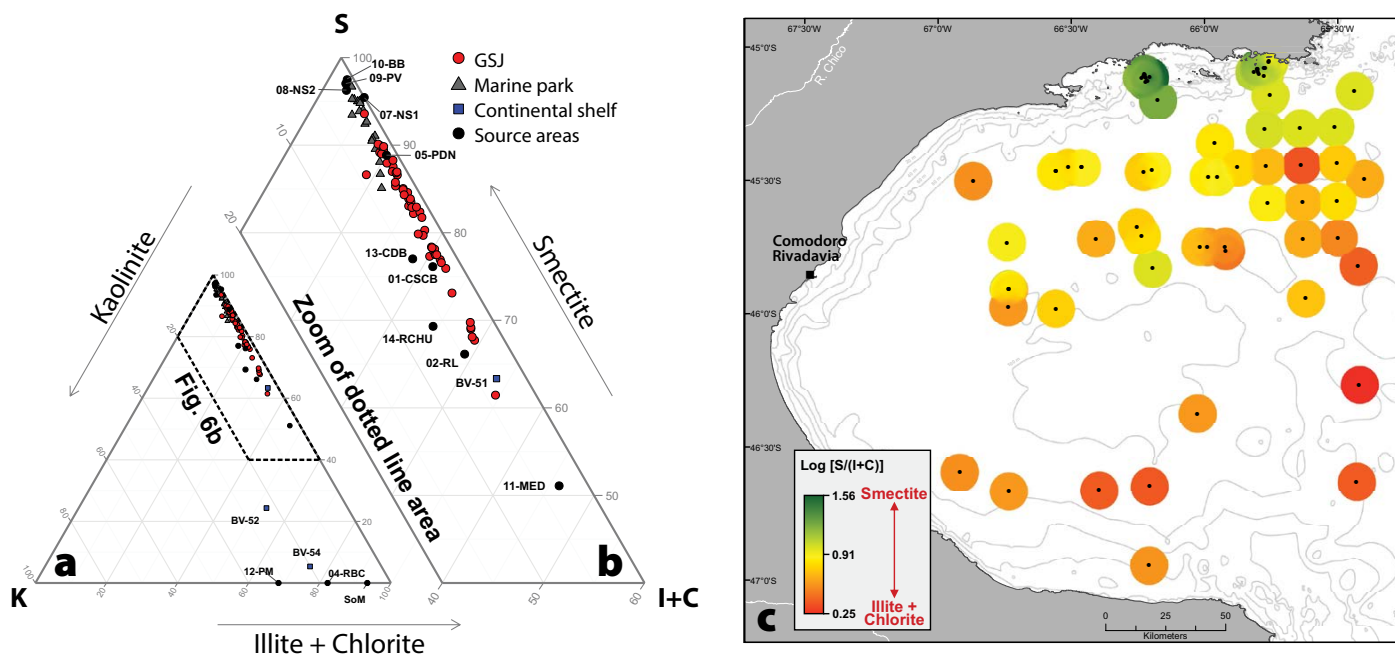


FIGURE 6. (a–b) Ternary diagram of smectite (S), kaolinite (K), and illite + chlorite (I+C) relative concentration in samples from marine park areas, other GSJ samples, continental shelf, and potential source areas. (c) Spatial distribution of $\log[S/(I+C)]$.

associated with EM3, which is characterized by a large dominant mode extending from medium silt to clay that could reflect a depositional environment associated with sediments transported over significant distances (e.g., currents and aeolian transport).

The bulk mineralogy, rather homogeneous and dominated by plagioclase, quartz, and clay minerals, is in accordance with the topsoil and riverine mineralogy from eastern Patagonia previously published in Gaiero et al. (2004). The high proportions of plagioclase and quartz reflect the dominant volcanic signature of Patagonia, mainly driven by the southern volcanic zone of the Andean Cordillera but also, to a lesser extent, by volcanic rocks erupted since the Jurassic. Indeed, numerous studies have highlighted the major influence of Andean volcanism on the mineralogical, chemical, and isotopic signatures of beach, riverine, and marine samples from western (Bertrand et al., 2012), as well as eastern Patagonia (Potter, 1994; Gaiero et al., 2007). The prevalence of clays in the riverine samples (Chubut and Deseado), as well as in samples from the area known as “Bajo de Sarmiento,” suggests that riverine and aeolian transports have an impact on the inputs of clays in the GSJ. According to Gaiero et al. (2004), the suspended loads of the Chubut and Deseado Rivers, likely to be partially transported to the gulf, present the highest proportions of clay minerals in comparison to other Patagonian riverine and topsoil samples. Furthermore, the potential of wind to transport clays from dust source areas such as Bajo de Sarmiento (Prospero et al., 2002; Montes et al., 2017) is reinforced by the nature of the soil covering the Gulf of San Jorge Basin. Indeed, the soil is mainly composed of yermosols that are often characterized by a developed argillic (clay) B horizon that is easily eroded by wind (Gut, 2008). In the GSJ, the sediments enriched in clay minerals are located in the deep and central areas that are associated with weaker hydrodynamic conditions and identified

as depositional environments (Fernández et al., 2003). In addition, the appreciable amounts of volcanoclastic particles, identified as rhyolitic tephra (Figure S2) in the bulk mineralogical composition and observed as glass shards in SEM images of the surface sediments (Figure S3b,c), also support the aeolian and riverine transport contribution, as opposed to coastal erosion, which carries modern and past (i.e., remobilization of terrestrial tephra deposits) volcanogenic particles into the GSJ. Furthermore, the geochemical composition of glass shards suggests a dominance of rhyolitic volcanoclastic material (Figure S3d); however, the sources of recent rhyolitic products are rare in the volcanic zone close to the GSJ (i.e., Southern Volcanic Zone of the Andes), except for the Chaitén volcano in Chile (López-Escobar et al., 1993). Thus, we hypothesize that the ash plumes generated by the explosive rhyolite eruptions of Chaitén volcano and the remobilization of associated tephra deposits represent the most conclusive source of modern tephra in the GSJ.

The well-defined correlation between the grain-size distribution and the bulk mineralogy, where the coarser grains are associated with clay-poor and plagioclase/quartz-rich samples (Figures 2 and 4a), highlights the presumptive impact of the grain size on the sediment mineral composition. Therefore, the bulk mineral composition of sediments in the GSJ is primarily controlled by the dominant and homogeneous continental volcanic signature in Patagonia, but it is also influenced by the grain-size distribution.

Our analysis of clay-mineral assemblages in the GSJ, highly dominated by smectite, is relatively consistent with the results reported both on the nearshore areas of Patagonia (Pierce and Siegel, 1979) and on the continent (i.e., riverine and topsoil material; Gaiero et al., 2004). This high smectite content is related to the combination of two factors: (1) potential high inputs of smectite from adjacent eastern and southern Patagonian sources (Petschick et al., 1996; Diekmann et al.,

2000), and (2) rapid gravitational settling on coastal areas of smectite compared to other clay minerals (Pierce and Siegel, 1979). Indeed, the well-crystallized smectite observed in the gulf (Table S2) is mostly connected to the physical weathering of Si-poor rocks, such as the basaltic and basalt-andesitic formations dominating the Cenozoic volcanism in the central part of Patagonia (Petschick et al., 1996; Corbella and Lara, 2008). Moreover, the smectite transported onto the Patagonian Shelf seems to be derived at selected locations from large morainic and glacio-fluvial Quaternary deposits (Marinoni et al., 1997). It should be noted that in the vicinity of the Gulf of San Jorge Basin, sedimentary and pyroclastic rocks represent potential sources of smectite (e.g., Las Flores Formation [Raigemborn et al., 2009]; Bajo Grande Formation [Dominguez et al., 2008]). Furthermore, because of the high proportions of smectite from the Bajo de Sarmiento (07NS1 and 08NS2) and the Deseado River (05PDN) samples, as well as its scattered proportions in the GSJ shore samples, the clay-mineral assemblages of riverine and terrestrial samples point to riverine and aeolian transport as the main suppliers of smectite to the gulf (Figure 6a,b).

The contrast between low to moderate proportions of illite and chlorite in the GSJ and higher contents in the shelf samples shows the influence of continental shelf inputs for these clay minerals in the gulf. The illite and chlorite are derived from Patagonian batholiths and low-grade metamorphic rocks located in Antarctica as well as in Patagonia (Petschick et al., 1996; Diekmann et al., 2000). The chlorite and illite are both transported from southern South America and the Drake Passage along the Argentinean continental shelf (Petschick et al., 1996). Once sediments settle on the shelf, the northward circulation controls their redistribution and transport (Palma et al., 2008). The inputs of illite and chlorite to the GSJ by the Patagonian Current flowing northward through the continental shelf from southern South America

are also supported by I+C enrichment in the eastern and southern parts of the gulf (Figure 6c).

In addition, the concentration of kaolinite in the gulf is very low despite the numerous outcrops of rhyolites and ignimbrites in eastern Patagonia, known as potential sources of residual kaolin deposits (Dominguez et al., 2008), and despite the significant amount of kaolinite in the Las Flores Formation, which overlies tablelands in some sectors of the San Jorge Gulf Basin (Raigemborn et al., 2009). This near absence of kaolinite may be due to dilution with much higher contents of smectite, illite, and chlorite.

The major and minor element composition of surface sediments seems well correlated to the mineralogical properties in the GSJ. The PC-1 scores derived from elemental geochemistry signatures show patterns of distribution similar to those found in the elemental balance of major mineral groups in the gulf. The large positive PC-1 scores are associated with Fe, Mg, and V in areas enriched in clays, and conversely, negative PC-1 scores are associated with Ca, Si, Sr, Zr, Mn, Al, K, and P in areas enriched in quartz and feldspar (Figures 5d and 4a). Furthermore, numerous major elements reveal good correlations with various minerals identified in the gulf. For example, the major components Si, Fe, and Ca are linked to the presence of quartz ($r^2 = 0.61$; Figure S4a), the sum of Fe-bearing minerals (notably, pyrite, magnetite, hematite, goethite, and maghemite) and clays ($r^2 = 0.66$; Figure S4d), and plagioclase ($r^2 = 0.77$, Figure S4b), respectively. The relationship between mineralogy and major element composition supports and strengthens the use of quantitative X-ray diffraction to determine the mineralogy of sediment samples, as well as the use of SedUnMix to estimate the proportions of potential sources for the composition of surface sediments in the GSJ. In addition, the absence of clear differences in the geochemical classification between particles from suspended sediments from the water column and surface sediments

from the same site reveals that most of the material carried toward the surface water of the gulf settle on the bottom of the GSJ (Figure 5c).

SUMMARY AND CONCLUSIONS

The investigation of grain size, bulk and clay mineralogy, and the geochemistry of surficial sediments from the GSJ was used to highlight the nature and spatial variability of surface sediments. The results reveal and allow quantification of numerous factors, such as continental volcanism, local coastal inputs (i.e., erosion and runoff), dust and aeolian transport, hydrodynamic conditions, and the northward-flowing Patagonian Current, that impact sedimentation in the GSJ. Based on our interpretation, coupled with nonlinear mixing models (SedUnMix) of

bulk mineralogy, we suggest that the origin of sediments in the GSJ is 50% from external/oceanic inputs, 40% from the inner gulf shores, and 10% from dust (i.e., aeolian transport). In the central part of the GSJ, a region associated with a lower-energy depositional environment enriched in clays (Figure 7), the contributions of external/oceanic and dust inputs increase to 60% and 15%, respectively, whereas inner gulf shore inputs decrease to 25%. The marine park area in the northeastern part of the GSJ constitutes an erosive environment linked to high proportions of quartz, plagioclase, and smectite (Figure 7), with a large contribution from the inner gulf shores (70%) to sediment composition. Furthermore, the southeastern part of the gulf can also be considered a distinct sedimentary

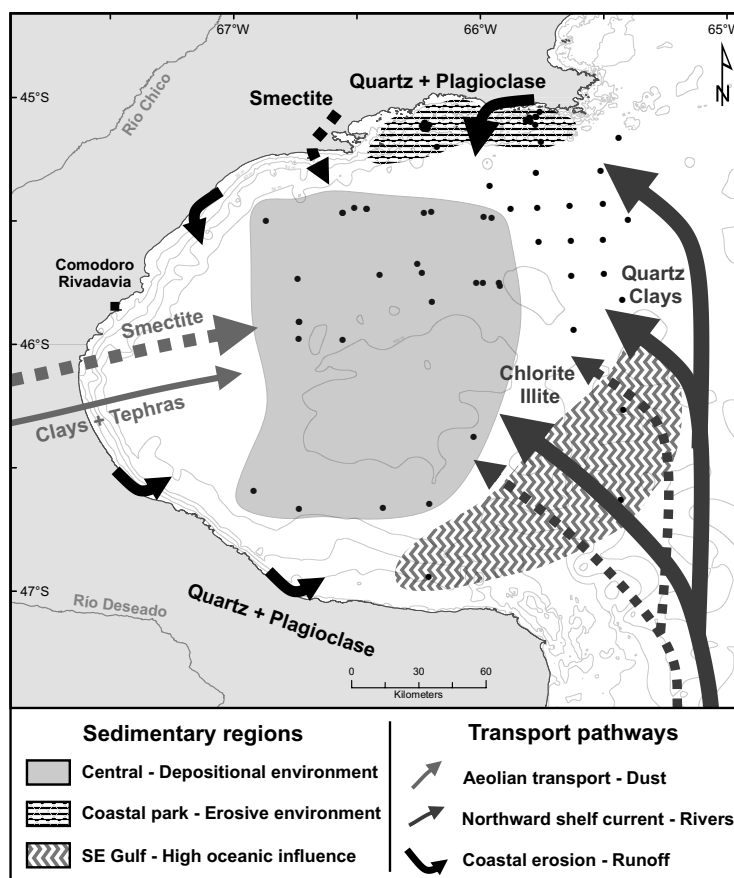



FIGURE 7. Schematic map of the main sedimentary regions and transport pathways identified in the Gulf of San Jorge area. The sedimentary regions were determined according to the authors' interpretations and previous results from Fernández et al. (2003). The bulk terrigenous inputs are illustrated with filled arrows, and the terrigenous clay inputs are depicted with dotted arrows. Note that the spatial distribution of the samples does not follow a regular and homogeneous pattern, leading to potentially underrepresented areas.

region enriched in quartz, illite, and chlorite minerals and highly influenced by external/oceanic inputs related to the northward-flowing continental shelf current (85%; Figure 7). Finally, in the absence of current major fluvial inputs, these results highlight the combined contributions of various sediment sources and transport mechanisms that must be taken into account when investigating recent and past sediment distributions and their interactions with biogeochemical processes in the GSJ. It is necessary to keep in mind that fluvial inputs were significant (Kokot, 2004) during past glaciations and deglaciations following sea level changes and glacial meltwater pulses, thus adding other possible sediment sources to the sedimentary budget during these periods. 

SUPPLEMENTARY MATERIALS

Supplementary materials are available online at <https://doi.org/10.5670/oceanog.2018.401>.

REFERENCES

- Andrews, J., G. Kristjánssdóttir, D.D. Eberl, and A. Jennings. 2013. A quantitative x-ray diffraction inventory of volcanoclastic inputs into the marine sediment archives off Iceland: A contribution to the Volcanoes in the Arctic System programme. *Polar Research* 32(1):1130, <https://doi.org/10.3402/polar.v32i0.11130>.
- Andrews, J.T., and C. Vogt. 2014. Source to sink: Statistical identification of regional variations in the mineralogy of surface sediments in the western Nordic Seas (58°N–75°N; 10°W–40°W). *Marine Geology* 357:151–162, <https://doi.org/10.1016/j.margeo.2014.08.005>.
- Bertrand, S., K.A. Huguen, J. Sepulveda, and S. Pantoja. 2012. Geochemistry of surface sediments from the fjords of Northern Chilean Patagonia (44–47°S): Spatial variability and implications for paleoclimate reconstructions. *Geochimica et Cosmochimica Acta* 76:125–146, <https://doi.org/10.1016/j.gca.2011.10.028>.
- Corbella, H., and L.E. Lara. 2008. Late Cenozoic quaternary volcanism in Patagonia and Tierra del Fuego. *Developments in Quaternary Sciences* 11:95–119, [https://doi.org/10.1016/S1571-0866\(07\)10006-3](https://doi.org/10.1016/S1571-0866(07)10006-3).
- Coronato, A.M., F. Coronato, E. Mazzoni, and M. Vázquez. 2008. The physical geography of Patagonia and Tierra del Fuego. *Developments in Quaternary Sciences* 11:13–55, [https://doi.org/10.1016/S1571-0866\(07\)10003-8](https://doi.org/10.1016/S1571-0866(07)10003-8).
- Crespi-Abril, A.C., A.M.I. Montes, G.N. Williams, and M.F. Carrasco. 2016. Uso de sensores remotos para la detección de eventos de transporte edáfico de sedimentos hacia ambientes marinos en Patagonia. *Meteorologica* 41(2):33–47.
- Crespi-Abril, A.C., G. Soria, A. De Cian, and C. López-Moreno. 2018. Roaring forties: An analysis of a decadal series of data of dust in Northern Patagonia. *Atmospheric Environment* 177:111–119, <https://doi.org/10.1016/j.atmosenv.2017.11.019>.
- Cuitiño, J.I., R.A. Scasso, R. Ventura Santos, and L.H. Mancini. 2015. Sr ages for the Chenque Formation in the Comodoro Rivadavia region (Golfo San Jorge Basin, Argentina): Stratigraphic implications. *Latin American Journal of Sedimentology and Basin Analysis* 22(1):13–28.
- de Mahiques, M.M., C.C.G. Tassinari, S. Marcolini, R.A. Violante, R.C.L. Figueira, I.C.A. da Silveira, L. Burone, and S.H. de Mello e Sousa. 2008. Nd and Pb isotope signatures on the Southeastern South American upper margin: Implications for sediment transport and source rocks. *Marine Geology* 250(1):51–63, <https://doi.org/10.1016/j.margeo.2007.11.007>.
- Diekmann, B., G. Kuhn, V. Rachold, A. Abelmann, U. Brathauer, D.K. Fütterer, R. Gersonde, and H. Grobe. 2000. Terrigenous sediment supply in the Scotia Sea (Southern Ocean): Response to Late Quaternary ice dynamics in Patagonia and on the Antarctic Peninsula. *Palaeogeography, Palaeoclimatology, Palaeoecology* 162(3):357–387, [https://doi.org/10.1016/S0031-0182\(00\)00138-3](https://doi.org/10.1016/S0031-0182(00)00138-3).
- Dominguez, E., C. Iglesias, and M. Dondi. 2008. The geology and mineralogy of a range of kaolins from the Santa Cruz and Chubut Provinces, Patagonia (Argentina). *Applied Clay Science* 40(1):124–142, <https://doi.org/10.1016/j.clay.2007.07.009>.
- Eberl, D.D. 2003. *User Guide to RockJock-A Program for Determining Quantitative Mineralogy from X-Ray Diffraction Data*. US Geological Survey, Open-File Report 03-78.
- Fernández, M., J.I. Carreto, J. Mora, and A. Roux. 2005. Physico-chemical characterization of the benthic environment of the Golfo San Jorge, Argentina. *Journal of the Marine Biological Association of the United Kingdom* 85(6):1,317–1,328, <https://doi.org/10.1017/S002531540501249X>.
- Fernández, M., A. Roux, E. Fernández, J. Caló, A. Marcos, and H. Aldacur. 2003. Grain-size analysis of surficial sediments from Golfo San Jorge, Argentina. *Journal of the Marine Biological Association of the United Kingdom* 83(6):1,193–1,197, <https://doi.org/10.1017/S0025315403008488>.
- Gaiero, D.M., F. Brunet, J.-L. Probst, and P.J. Depetris. 2007. A uniform isotopic and chemical signature of dust exported from Patagonia: Rock sources and occurrence in southern environments. *Chemical Geology* 238:107–120, <https://doi.org/10.1016/j.chemgeo.2006.11.003>.
- Gaiero, D.M., P.J. Depetris, J.-L. Probst, S.M. Bidart, and L. Leleyter. 2004. The signature of river- and wind-borne materials exported from Patagonia to the southern latitudes: A view from REEs and implications for paleoclimatic interpretations. *Earth and Planetary Science Letters* 219(3):357–376, [https://doi.org/10.1016/S0012-821X\(03\)00686-1](https://doi.org/10.1016/S0012-821X(03)00686-1).
- Gaiero, D.M., J.-L. Probst, P.J. Depetris, S.M. Bidart, and L. Leleyter. 2003. Iron and other transition metals in Patagonian riverborne and windborne materials: geochemical control and transport to the southern South Atlantic Ocean. *Geochimica et Cosmochimica Acta* 67(19):3,603–3,623, [https://doi.org/10.1016/S0016-7037\(03\)00211-4](https://doi.org/10.1016/S0016-7037(03)00211-4).
- Gamboa, A., J. Montero-Serrano, G. St-Onge, A. Rochon, and P.-A. Desjage. 2017. Mineralogical, geochemical, and magnetic signatures of surface sediments from the Canadian Beaufort Shelf and Amundsen Gulf (Canadian Arctic). *Geochemistry, Geophysics, Geosystems* 18(2):488–512, <https://doi.org/10.1002/2016GC006477>.
- Gut, B. 2008. Geology, climate and soils of Patagonia. Pp. 9–18 in *Trees in Patagonia*. Springer Science & Business Media.
- Herron, M.M. 1988. Geochemical classification of terrigenous sands and shales from core or log data. *Journal of Sedimentary Research* 58(5):820–829, <https://doi.org/10.1306/212F8E77-2B24-11D7-8648000102C1865D>.
- Isla, F.I., N. Iantanos, and E. Estrada. 2002. Playas reflectivas y disipativas macromarales del Golfo San Jorge, Chubut. *Revista de La Asociación Argentina de Sedimentología* 9(2):155–164.
- Kilian, R., and F. Lamy. 2012. A review of glacial and Holocene paleoclimate records from southernmost Patagonia (49–55°S). *Quaternary Science Reviews* 53:1–23, <https://doi.org/10.1016/j.quascirev.2012.07.017>.
- Kokot, R.R. 2004. Erosión en la costa patagónica por cambio climático. *Revista de La Asociación Geológica Argentina* 59(4):715–726.
- López-Escobar, L., R. Kilian, P.D. Kempton, and M. Tagiri. 1993. Petrography and geochemistry of Quaternary rocks from the Southern Volcanic Zone of the Andes between 41°30' and 46°00'S, Chile. *Andean Geology*, 20(1):33–55.
- Marinoni, L., M. Setti, and F. Soggetti. 1997. Mineralogy of sea-bottom sediments from the Strait of Magellan. *Boletino di Geofisica Teorica ed Applicata* 38:281–292.
- Martínez, O.A., and A. Kutschker. 2011. The “Rodados Patagónicos” (Patagonian shingle formation) of eastern Patagonia: Environmental conditions of gravel sedimentation. *Biological Journal of the Linnean Society* 103(2):336–345, <https://doi.org/10.1111/j.1095-8312.2011.01651.x>.
- Montes, A., S.S. Rodríguez, and C.E. Domínguez. 2017. Geomorphology context and characterization of dune fields developed by the southern westerlies at drying Colhué Huapi shallow lake, Patagonia Argentina. *Aeolian Research* 28:58–70, <https://doi.org/10.1016/j.aeolia.2017.08.001>.
- Montes, A., S. Rodríguez, C. San Martín, and J. Allard. 2015. Migración de campos de dunas en cañadones costeros de Patagonia: Geomorfología e implicaciones paleoclimáticas. *Revisita de La Sociedad Geologica de España* 28(2):65–76.
- Nagai, R.H., P.A.L. Ferreira, S. Mulkherjee, M.V. Martins, R.C.L. Figueira, S.H.M. Sousa, and M.M. Mahiques. 2014. Hydrodynamic controls on the distribution of surface sediments from the southeast South American continental shelf between 23°S and 38°S. *Continental Shelf Research* 89:51–60, <https://doi.org/10.1016/j.csr.2013.09.016>.
- Palma, E.D., R.P. Matano, and A.R. Piola. 2008. A numerical study of the Southwestern Atlantic Shelf circulation: Stratified ocean response to local and offshore forcing. *Journal of Geophysical Research* 113(C11), <https://doi.org/10.1029/2007JC004720>.
- Pankhurst, R.J., P.T. Leat, P. Sruoga, C.W. Rapela, M. Márquez, B.C. Storey, and T.R. Riley. 1998. The Chon Aike province of Patagonia and related rocks in West Antarctica: A silicic large igneous province. *Journal of Volcanology and Geothermal Research* 81(1):113–136, [https://doi.org/10.1016/S0377-0273\(97\)00070-X](https://doi.org/10.1016/S0377-0273(97)00070-X).
- Petschick, R., G. Kuhn, and F. Gingele. 1996. Clay mineral distribution in surface sediments of the South Atlantic: Sources, transport, and relation to oceanography. *Marine Geology* 130(3):203–229, [https://doi.org/10.1016/0025-3227\(95\)00148-4](https://doi.org/10.1016/0025-3227(95)00148-4).
- Pierce, J.W., and F.R. Siegel. 1979. Suspended particulate matter on the southern Argentine shelf. *Marine Geology* 29(1):73–91, [https://doi.org/10.1016/0025-3227\(79\)90103-8](https://doi.org/10.1016/0025-3227(79)90103-8).
- Potter, P.E. 1994. Modern sands of South America: Composition, provenance and global significance. *Geologische Rundschau* 83(1):212–232, <https://doi.org/10.1007/BF00211904>.

- Preda, M., and M.E. Cox. 2005. Chemical and mineralogical composition of marine sediments, and relation to their source and transport, Gulf of Carpentaria, Northern Australia. *Journal of Marine Systems* 53(1):169–186, <https://doi.org/10.1016/j.jmarsys.2004.05.003>.
- Prospero, J.M., P. Ginoux, O. Torres, S.E. Nicholson, and T.E. Gill. 2002. Environmental characterization of global sources of atmospheric soil dust identified with the Nimbus 7 Total Ozone Mapping Spectrometer (TOMS) absorbing aerosol product. *Reviews of Geophysics* 40(1):2–31, <https://doi.org/10.1029/2000RG000095>.
- Raigemborn, M., M. Brea, A. Zucol, and S. Matheos. 2009. Early Paleogene climate at mid latitude in South America: Mineralogical and paleobotanical proxies from continental sequences in Golfo San Jorge basin (Patagonia, Argentina). *Geologica Acta: An International Earth Science Journal* 7(1–2):125–145, <https://doi.org/10.1344/105.000000269>.
- Saukel, C., R. Stein, C. Vogt, and V.P. Shevchenko. 2010. Clay-mineral and grain-size distributions in surface sediments of the White Sea (Arctic Ocean): Indicators of sediment sources and transport processes. *Geo-Marine Letters* 30(6):605–616, <https://doi.org/10.1007/s00367-010-0210-2>.
- Spagnoli, F., G. Bartholini, E. Dinelli, and P. Giordano. 2008. Geochemistry and particle size of surface sediments of Gulf of Manfredonia (Southern Adriatic Sea). *Estuarine, Coastal and Shelf Science* 80(1):21–30, <https://doi.org/10.1016/j.ecss.2008.07.008>.
- Sylwan, C.A. 2001. Geology of the Golfo San Jorge Basin, Argentina. *Geología de la Cuenca del Golfo San Jorge, Argentina. Journal of Iberian Geology* 27:123–158.
- Violante, R.A., C.M. Paterlini, S.I. Marcolini, I.P. Costa, J.L. Cavallotto, C. Laprida, W. Dragani, N.G. Chapori, S. Watanabe, and V. Totah. 2014. The Argentine continental shelf: Morphology, sediments, processes and evolution since the Last Glacial Maximum. *Geological Society, London, Memoirs* 41(1):55–68, <https://doi.org/10.1144/M41.6>.

ACKNOWLEDGMENTS

The authors would like to sincerely thank the captain, crew, and scientific participants of the COR1404 (MARES and MARGES) expedition on board the R/V *Coriolis II*. Financial support for MARES and MARGES expeditions was provided by the Ministerio de Ciencia, Tecnología e Innovación Productiva (MINCYT), Provincia de Chubut and Consejo Nacional de Investigaciones Científicas y Técnicas (CONICET). This research was funded by the Natural Sciences and Engineering Research Council of Canada (NSERC) through Discovery grants to G. St-Onge and J.-C. Montero-Serrano and by the Fond de recherche du Québec – Nature et Technologies (FRQNT) through a team grant to G. St-Onge, J.-C. Montero-Serrano, and A. Rochon. We also acknowledge the financial support of the Canadian Foundation for Innovation (CFI) and Economic Development Canada for the acquisitions of the PANalytical X-ray diffractometer (X'Pert Powder) and the X-ray fluorescence (Epsilon 3-XL), respectively. We acknowledge the use of imagery from the NASA Worldview application (<https://worldview.earthdata.nasa.gov/>) operated by the NASA/Goddard Space Flight Center Earth Science Data and Information System (ESDIS) project. The authors thank Pierre Larouche of Fisheries and Oceans Canada for providing water column samples. We are thankful to Claude Belzile and Quentin Beauvais (UQAR-ISMER) for SEM image acquisition and technical support. Finally, we are grateful to reviewers John T. Andrews and Federico Spagnoli for their constructive reviews.

AUTHORS

Pierre-Arnaud Desiage (desiage.pierre.arnaud@gmail.com) is PhD student and **Jean-Carlos Montero-Serrano** is Professor, both at the Institut des sciences de la mer de Rimouski, Université du Québec à Rimouski, Rimouski, Québec, Canada. **Guillaume St-Onge** is Professor and Canada Research Chair in Marine Geology, Institut des sciences de la mer de Rimouski, Université du Québec à Rimouski, Rimouski, Québec, Canada. **Augusto César Crespi-Abril** is Associate Professor, Universidad Nacional de la Patagonia San Juan Bosco (UNPSJB), Puerto Madryn, Argentina, and Research Scientist, Centro para el Estudio de los Sistemas Marinos, Centro Nacional Patagónico (CENPAT), Consejo Nacional de Investigaciones Científicas y Técnicas (CONICET), Puerto Madryn, Argentina. **Erica Giarratano** is Research Scientist CENPAT, CONICET, Puerto Madryn, Argentina. **Mónica Noemí Gil** is Associate Professor, UNPSJB, Puerto Madryn, Argentina, and Senior Professional CENPAT, CONICET, Puerto Madryn, Argentina. **Miguel J. Haller** is Professor Emeritus UNPSJB, Puerto Madryn, Argentina, and Senior Researcher CENPAT, CONICET, Puerto Madryn, Argentina.

ARTICLE CITATION

Desiage, P.-A., J.-C. Montero-Serrano, G. St-Onge, A.C. Crespi-Abril, E. Giarratano, M.N. Gil, and M.J. Haller. 2018. Quantifying sources and transport pathways of surface sediments in the Gulf of San Jorge, central Patagonia (Argentina). *Oceanography* 31(4), <https://doi.org/10.5670/oceanog.2018.401>.

METHODS

Prior to the grain size, bulk mineralogical, and geochemical analyses, samples (<2 mm) were pretreated with 10 ml of hydrogen peroxide (H₂O₂; 30%) and 10 ml of hydrochloric acid (HCl; 0.5 N) for at least 72 hours to remove organic matter and biogenic carbonate. Next, an aliquot of this sediment sample was ground using a micronizing mill (McCrone) and 5 ml of ethanol for approximately 10 minutes until a homogeneous mixture of grain <10 µm was obtained. The mixture was oven-dried at 60°C and ground again in an agate mortar to prevent aggregations of fine particles due to drying. Aliquots of these homogenized sediment samples were used for bulk mineralogical and geochemical analyses.

The observations of tephra using a JEOL 6460LV SEM were performed on the 300–63 µm and <63 µm fractions of the BV01, BV06, and BC11 samples. Before sieving, the samples were pretreated with 10 ml of hydrogen peroxide (H₂O₂; 30%) for 24 hours and rinsed with distilled water at least five times. Finally, the samples were oven-dried at 60°C.

GRAIN-SIZE ANALYSIS

The grain-size analysis of sediment samples was carried out on detrital fraction using a Beckman Coulter Particle Size Analyzer LS 13 320 (0.04–2,000 µm). Deflocculation was performed by successive washing with distilled water and the samples were mechanically shaken for 12 hours before measurement. Grain-size distribution and statistical parameters were processed with the GRADISTAT software using the geometric (µm) and logarithmic (φ) method of moments (Blott and Pye, 2001). The end-member modeling algorithm (EMMA; Dietze et al., 2012) was applied to the grain-size data. The EMMA algorithm is used to unmix the original grain-size distribution (Figure 2b) in order to extract meaningful EM grain-size distributions and thus

to estimate the processes (transport conditions) related to the EM grain-size distributions (Dietze et al., 2012). The characteristics and detailed procedures of the EMMA method used for this study are presented in Dietze et al. (2012) and Dietze and Dietze (2013).

SOURCE SAMPLES

In order to quantify potential sources of sediment in the GSJ, 13 terrestrial and riverine samples were retrieved in August 2016 (Figure 1a,b); nine of them were collected on the shore of the GSJ (topsoil and beach sediments), two at the mouths of the Chubut and Deseado Rivers (river bank and beach sediments, respectively), and two in the Bajo de Sarmiento area (topsoil sediments from the dry bed of Lake Colhué Huapí [NS1] and 10 km to the east of the lake, close to dune fields formed by the southern westerlies [NS2; Montes et al., 2017]). A marine surface sediment sample (0–2 cm sediment depth) from Magellan Strait was also analyzed. The latter was recovered with a CASQ gravity corer (MD07-3131) during the MD 159 PACHIDERME expedition on board R/V *Marion Dufresne II* (Figure 1a; February 2007).

BULK MINERAL ANALYSIS

The random powder samples were side-loaded into holders and analyzed by X-ray diffraction (XRD) using a PANalytical X'Pert Powder diffractometer. The samples were measured between 5° and 65° 2θ in steps of 0.02° and a counting time of 2 seconds per step. Bulk mineral associations were analyzed following the quantitative method developed by Eberl (2003) and Eberl and Smith (2009) and used in other Late Quaternary marine studies that deal with sediment mineralogy (e.g., Andrews et al., 2015, 2016; Andrews and Vogt 2014). For the quantification of the major mineralogical components, the XRD scans were converted into mineral

weight percentages (wt.%) using the standardless option of the Excel macro-program Rockjock v11 (Eberl, 2003; Eberl and Smith, 2009). This program uses a full-pattern fitting method that permits the quantification of the whole-sediment mineralogy with an error of approximately ±3 wt% at 50 wt% of a mineral (Eberl, 2003). To verify the quality of this fitting procedure, a degree-of-fit (DOF = minimum absolute difference) statistic was calculated between the measured and simulated XRD patterns. The DOF values obtained with our samples were satisfying. They were within a range of 0.072 to 0.442 with an average of 0.165 for the 95 samples. Polytypes of illite, smectite, plagioclase feldspars, and K-feldspars are reported as a total amount (e.g., Andrews and Vogt, 2014; Andrews et al., 2015, 2016). This qXRD method came in second in the international “Reynolds Cup” quantitative mineral analysis competition (Omotoso et al., 2006). The calculated total mineral wt% was normalized to sum to 100%. We present the wt % data for 12 minerals (Table S2), but we focus on 11 minerals and exclude carbonates and biotite because of their restricted occurrence (Table S5).

Likewise, we used the nonlinear unmixing Excel macro program SedUnMixMC (Andrews and Eberl, 2012; Andrews et al., 2015, 2016) to obtain a quantitative understanding of the surface changes in sediment provenance. We ran SedUnMixMC on the normalized (100%) data for the 11 key minerals (Table S5) that represented more than 99% of the overall mineral concentration in the sediment samples. SedUnMixMC allows up to six sources to be examined as potential contributors to sediment composition. Based on surface geology (e.g., Pankhurst and Rapela, 1995; Pankhurst et al., 1998; see Physical Setting section in main text) and sediment transport pathways (e.g., Matano

et al., 2010; Montes et al., 2017; see Physical Setting and Sedimentation sections in main text), we suggest that the surface sediment compositions in the GSJ are potentially the mixing product of five source areas: (S1) Marine park sector (i.e., rhyolitic rocks outcrop), (S2) Other coastal areas of the GSJ (i.e., cliffs and beaches of Eocene-Miocene sedimentary rocks and/or Quaternary fluvio-glacial deposits), (S3) rivers (i.e., Chubut and Deseado, as well as Strait of Magellan), (S4) dust from continental Patagonia (i.e., Bajo de Sarmiento area), and (S5) continental shelf (i.e., southern South America influence and northward shelf Patagonian Current). Under this context, SedUnMix was run using five sources, and each source is represented by two to five of the source area samples (Table S5). The samples were attributed to potential sources according to their locations coupled with geological and environmental context, and also with the results from the mineralogical analysis (Figure 3).

CLAY MINERAL ANALYSIS

In this paper, clay minerals were quantified in the bulk sediment fraction (<2 mm) using the Excel macro program RockJock. However, nearly all previous clay-mineral provenance studies of the Argentinean continental shelf used oriented mounts of the <2 μm sediment fraction to identify and semi-quantify the clay-mineral abundance, notably illite, kaolinite, chlorite, and smectite (e.g., Petschick et al., 1996; Diekmann et al., 2000; Dominguez et al., 2008). Therefore, in this study, the clay-size fraction of all sediment samples was isolated and analyzed in this manner for comparison. Clay mineral associations were studied using XRD following established protocols (Bout-Roumazeilles et al., 1999). The clay-sized fraction (<2 μm) was isolated by settling according to Stoke's Law, concentrated by centrifugation, and oriented on glass slides. For each sample, analyses were performed on three subsamples under different conditions: (1) untreated sample (normal run); (2)

ethylene-glycol saturation applied for 12 hours (glycol run); and (3) sample heated at 490°C for two hours (heating run). The analyses were measured on a PANalytical X'Pert Powder diffractometer, between 2.49° and 32.49° 2 θ for the normal and glycol runs and between 2.49° and 14.5° 2 θ for the heating run, with steps of 0.02° and a counting time of three seconds per step for all the runs. Semi-quantitative estimation of clay mineral abundances (smectite, illite, chlorite, kaolinite, and illite/smectite mixed layer) based on peak areas was performed using the MacDiff® 4.2.5 software (Petschick, 2000). The error on the reproducibility of measurements is estimated to be 5% for each clay mineral, as verified with analyses on replicate samples. Note that the comparison of both RockJock and oriented mounted methods yielded similar results within analytical uncertainty (Figure S5). This highlights the robustness of the qXRD method used in our study.

BULK ELEMENTAL GEOCHEMISTRY

Concentrations of 14 major and minor elements (Al₂O₃, SiO₂, K₂O, MgO, CaO, TiO₂, MnO, Fe₂O₃, P₂O₅, Sr, V, Cr, Zn, and Zr) were measured by energy dispersive X-ray fluorescence spectrometry (EDXRF) using a PANalytical Epsilon 3-XL. Before EDXRF analysis, loss on ignition (LOI) was determined gravimetrically by heating the dried samples up to 950°C for two hours. Subsequently, the glass disks were made by melting ~0.6 g of samples with a mixture of lithium tetraborate and metaborate (49.75% Li₂B₄O₇, 49.75% LiBO₂, and 0.5% LiBr, CLAISSE) in an automated fusion furnace (CLAISSE M4 Fluxer) prior to being analyzed with the spectrometer. Acquired XRF spectra were processed with the standardless Omnia software package (PANalytical). Analytical accuracy, based on both an international standard (USGS SDC-1) and analysis of replicate samples, was about 1%–5% for major elements and 5%–10% for the other elements.

Likewise, the elemental composition

analysis of filters and tephtras was performed using an INCA X-sight energy dispersive X-ray spectrometer (Oxford Instruments) coupled to a JEOL 6460LV scanning electron microscope. X-ray spectra were measured from 15 randomly chosen particles for filters and 10 glass shard fragments for tephtras, with two or three spectra per particle. Each spectrum was acquired for 60 (filters) and 120 (tephtras) seconds of live time at an accelerating voltage of 20 kV. System quantitative optimization was made using copper as standard.

The relative proportions of the three most abundant detrital elements (Si, Al, and Fe) of the GSJ samples are presented in the form of a ternary diagram with respective mean grain sizes using the phi-scale to determine the influence of grain size on major element composition. In addition, the ternary plot Fe-K-Ca was used here to understand the contributions of various Patagonian sedimentary sources to the elemental geochemistry of sediments in the GSJ (see Bulk Mineralogy section in the main text). In this diagram the GSJ samples (excluding marine park sites) are illustrated according to their locations in the gulf.

STATISTICAL APPROACH

The mineralogical and geochemical data are of a compositional nature, that is, they are vectors of non-negative values subjected to a constant-sum constraint (usually 100%). This implies that relevant information is contained in the relative magnitudes, so statistical analysis must focus on the ratios between components (Aitchison, 1986). Under this framework, the discriminant scatter plots based on mineralogical and geochemical data were represented here as log ratios. Note that a log transformation will reduce the very high values and spread out the small data values and is therefore well suited for right-skewed distributions (van den Boogaart and Tolosana-Delgado, 2013). Thus, compared to the raw data, the log-ratio scatter plots exhibit better sediment discrimination. Likewise, in order

to visualize the main tendencies of mineralogical enrichment in the gulf, the spatial distribution of the major mineral groups were represented as mineralogical balances (i.e., $b\{(\text{Quartz}+\text{Feldspars})/\text{Clays}\}$). Note that mineralogical balances are log contrasts resulting from a log ratio of two geometric means of two non-overlapping mineralogical groups (Egozcue and Pawlowsky-Glahn, 2005). Furthermore, a principal component analysis (PCA) was performed on the elemental geochemical data set in order to highlight elemental associations with similar relative variation patterns that may be interpreted from an environmental standpoint (e.g., Montero-Serrano et al., 2010). Prior to all multivariate analyses, a log-centered (clr) transform was applied to the data (Aitchison, 1990). The clr transform is derived by dividing each variable (e.g., mineral percentage, element concentrations) by the geometric mean of the composition of the individual observations and then taking the logarithm. This operation removes statistical constraints on compositional variables, such as the constant-unit sum, and allows the valid application of classical (Euclidean) statistical methods to compositional data (Aitchison, 1990; Montero-Serrano et al., 2010). Statistical calculations were conducted with CoDaPack v2.02.04 (Thió-Henestrosa and Martín-Fernández, 2005) and “R” software using the packages “compositions” (van den Boogaart and Tolosana-Delgado, 2008) and “vegan” (Oksanen et al., 2016). Finally, the spatial interpolations of the results from bulk and clay mineralogy and elemental geochemistry were generated using the inverse distance weighting (IDW) algorithm available in ArcGIS® Spatial Analyst Tools.

REFERENCES

- Aitchison, J. 1986. *The Statistical Analysis of Compositional Data*. Chapman and Hall, London, 416 pp.
- Aitchison, J. 1990. Relative variation diagrams for describing patterns of compositional variability. *Mathematical Geology* 22(4):487–511, <https://doi.org/10.1007/BF00890330>.
- Andrews, J.T., A.A. Björk, D.D. Eberl, A.E. Jennings, and E.P. Verplanck. 2015. Significant differences in late Quaternary bedrock erosion and transport: East versus West Greenland ~70° N: Evidence from the mineralogy of offshore glacial marine sediments. *Journal of Quaternary Science* 30(5):452–463, <https://doi.org/10.1002/jqs.2787>.
- Andrews, J., and D.D. Eberl. 2012. Determination of sediment provenance by unmixing the mineralogy of source-area sediments: The “SedUnMix” program. *Marine Geology* 291:24–33, <https://doi.org/10.1016/j.margeo.2011.10.007>.
- Andrews, J.T., R. Stein, M. Moros, and K. Perner. 2016. Late Quaternary changes in sediment composition on the NE Greenland margin (~73°N) with a focus on the fjords and shelf. *Boreas* 45(3):381–397, <https://doi.org/10.1111/bor.12169>.
- Andrews, J.T., and C. Vogt. 2014. Source to sink: Statistical identification of regional variations in the mineralogy of surface sediments in the western Nordic Seas (58°N–75°N; 10°W–40°W). *Marine Geology* 357:151–162, <https://doi.org/10.1016/j.margeo.2014.08.005>.
- Blott, S.J., and K. Pye. 2001. GRADISTAT: A grain size distribution and statistics package for the analysis of unconsolidated sediments. *Earth Surface Processes and Landforms* 26(11):1,237–1,248, <https://doi.org/10.1002/esp.261>.
- Bout-Roumazeilles, V., E. Cortijo, L. Labeyrie, and P. Debrabant. 1999. Clay mineral evidence of nepheloid layer contributions to the Heinrich layers in the northwest Atlantic. *Palaeogeography, Palaeoclimatology, Palaeoecology* 146(1):211–228, [https://doi.org/10.1016/S0031-0182\(98\)00137-0](https://doi.org/10.1016/S0031-0182(98)00137-0).
- Carel, M., G. Siani, and G. Delpech. 2011. Tephrostratigraphy of a deep-sea sediment sequence off the south Chilean margin: New insight into the Hudson volcanic activity since the last glacial period. *Journal of Volcanology and Geothermal Research* 208(3):99–111, <https://doi.org/10.1016/j.jvolgeores.2011.09.011>.
- Diekmann, B., G. Kuhn, V. Rachold, A. Abelmann, U. Brathauer, D. K. Fütterer, R. Gersonde, and H. Grobe. 2000. Terrigenous sediment supply in the Scotia Sea (Southern Ocean): Response to Late Quaternary ice dynamics in Patagonia and on the Antarctic Peninsula. *Palaeogeography, Palaeoclimatology, Palaeoecology* 162(3):357–387, [https://doi.org/10.1016/S0031-0182\(00\)00138-3](https://doi.org/10.1016/S0031-0182(00)00138-3).
- Dietze, M., and E. Dietze. 2013. EMMAgeo: End-member modelling algorithm and supporting functions for grain-size analysis. R package version 0.91, <https://cran.r-project.org/web/packages/EMMAgeo/index.html>.
- Dietze, E., K. Hartmann, B. Diekmann, J. Jmker, F. Lehmkühn, S. Opitz, G. Stauch, B. Wünnemann, and A. Borchers. 2012. An end-member algorithm for deciphering modern detrital processes from lake sediments of Lake Donggi Cona, NE Tibetan Plateau, China. *Sedimentary Geology* 243–244:169–180, <https://doi.org/10.1016/j.sedgeo.2011.09.014>.
- Dominguez, E., C. Iglesias, and M. Dondi. 2008. The geology and mineralogy of a range of kaolins from the Santa Cruz and Chubut Provinces, Patagonia (Argentina). *Applied Clay Science* 40(1):124–142, <https://doi.org/10.1016/j.clay.2007.07.009>.
- Eberl, D.D. 2003. *User Guide to RockJock-A Program for Determining Quantitative Mineralogy from X-Ray Diffraction Data*. US Geological Survey, Open-File Report 03-78.
- Eberl, D.D., and D.B. Smith. 2009. Mineralogy of soils from two continental-scale transects across the United States and Canada and its relation to soil geochemistry and climate. *Applied Geochemistry* 24(8):1,394–1,404, <https://doi.org/10.1016/j.apgeochem.2009.04.010>.
- Egozcue, J.J., and V. Pawlowsky-Glahn. 2005. Groups of parts and their balances in compositional data analysis. *Mathematical Geology* 37(7):795–828, <https://doi.org/10.1007/s11004-005-7381-9>.
- Matano, R., E.D. Palma, and A.R. Piola. 2010. The influence of the Brazil and Malvinas Currents on the southwestern Atlantic shelf circulation. *Ocean Science* 6:983–995, <https://doi.org/10.5194/os-6-983-2010>.
- Montero-Serrano, J.C., J. Palarea-Albaladejo, J.A. Martín-Fernández, M. Martínez-Santana, and J.V. Gutiérrez-Martín. 2010. Sedimentary chemofacies characterization by means of multivariate analysis. *Sedimentary Geology* 228(3):218–228, <https://doi.org/10.1016/j.sedgeo.2010.04.013>.
- Montes, A., S.S. Rodríguez, and C.E. Domínguez. 2017. Geomorphology context and characterization of dunefields developed by the southern westerlies at drying Colhué Huapi shallow lake, Patagonia Argentina. *aeolian Research* 28:58–70, <https://doi.org/10.1016/j.aeolia.2017.08.001>.
- Oksanen, J., F.G. Blanchet, R. Kindt, P. Legendre, P.R. Minchin, R.B. O’Hara, G.L. Simpson, P. Solymos, M.H.H. Stevens, and H. Wagner. 2016. *vegan: Community Ecology Package*, version 2.4-1, <https://cran.r-project.org/web/packages/vegan/index.html>.
- Omotoso, O., D.K. McCarty, S. Hillier, and R. Kleeberg. 2006. Some successful approaches to quantitative mineral analysis as revealed by the 3rd Reynolds Cup contest. *Clays and Clay Minerals* 54(6):748–760, <https://doi.org/10.1346/CCMN.2006.0540609>.
- Pankhurst, R.J., P.T. Leat, P. Sruoga, C.W. Rapela, M. Márquez, B.C. Storey, and T.R. Riley. 1998. The Chon Aike province of Patagonia and related rocks in West Antarctica: A silicic large igneous province. *Journal of Volcanology and Geothermal Research* 81(1):113–136, [https://doi.org/10.1016/S0377-0273\(97\)00070-X](https://doi.org/10.1016/S0377-0273(97)00070-X).
- Pankhurst, R.J., and C.W. Rapela. 1995. Production of Jurassic rhyolite by anatexis of the lower crust of Patagonia. *Earth and Planetary Science Letters* 134:23–36, [https://doi.org/10.1016/0012-821X\(95\)00103-J](https://doi.org/10.1016/0012-821X(95)00103-J).
- Petschick, R. 2000. MacDiff 4.2.5 Manual, <http://www.geol-pal.uni-frankfurt.de/Staff/Hompages/Petschick/classicsoftware.html>.
- Petschick, R., G. Kuhn, and F. Gingele. 1996. Clay mineral distribution in surface sediments of the South Atlantic: Sources, transport, and relation to oceanography. *Marine Geology* 130(3):203–229, [https://doi.org/10.1016/0025-3227\(95\)00148-4](https://doi.org/10.1016/0025-3227(95)00148-4).
- Ruggieri, F., J.L. Fernandez-Turiel, J. Saavedra, D. Gimeno, E. Polanco, A. Amigo, G. Galindo, and A. Caselli. 2012. Contribution of volcanic ashes to the regional geochemical balance: The 2008 eruption of Chaitén volcano, Southern Chile. *Science of the Total Environment* 425:75–88, <https://doi.org/10.1016/j.scitotenv.2012.03.011>.
- Thió-Henestrosa, S., and J.A. Martín-Fernández. 2005. Dealing with compositional data: The freeware CoDaPack. *Mathematical Geology* 37(7):773–793, <https://doi.org/10.1007/s11004-005-7379-3>.
- van den Boogaart, K.G., and R. Tolosana-Delgado. 2008. “compositions”: A unified R package to analyze compositional data. *Computers & Geosciences* 34(4):320–338, <https://doi.org/10.1016/j.cageo.2006.11.017>.
- van den Boogaart, K.G., and R. Tolosana-Delgado. 2013. *Analyzing Compositional Data with R*. Springer, Heidelberg-New York-Dordrecht-London, 273 pp.
- Watt, S.F.L., D.M. Pyle, T.A. Mather, R.S. Martin, and N.E. Matthews. 2009. Fallout and distribution of volcanic ash over Argentina following the May 2008 explosive eruption of Chaitén, Chile. *Journal of Geophysical Research* 114(B4), <https://doi.org/10.1029/2008JB006219>.

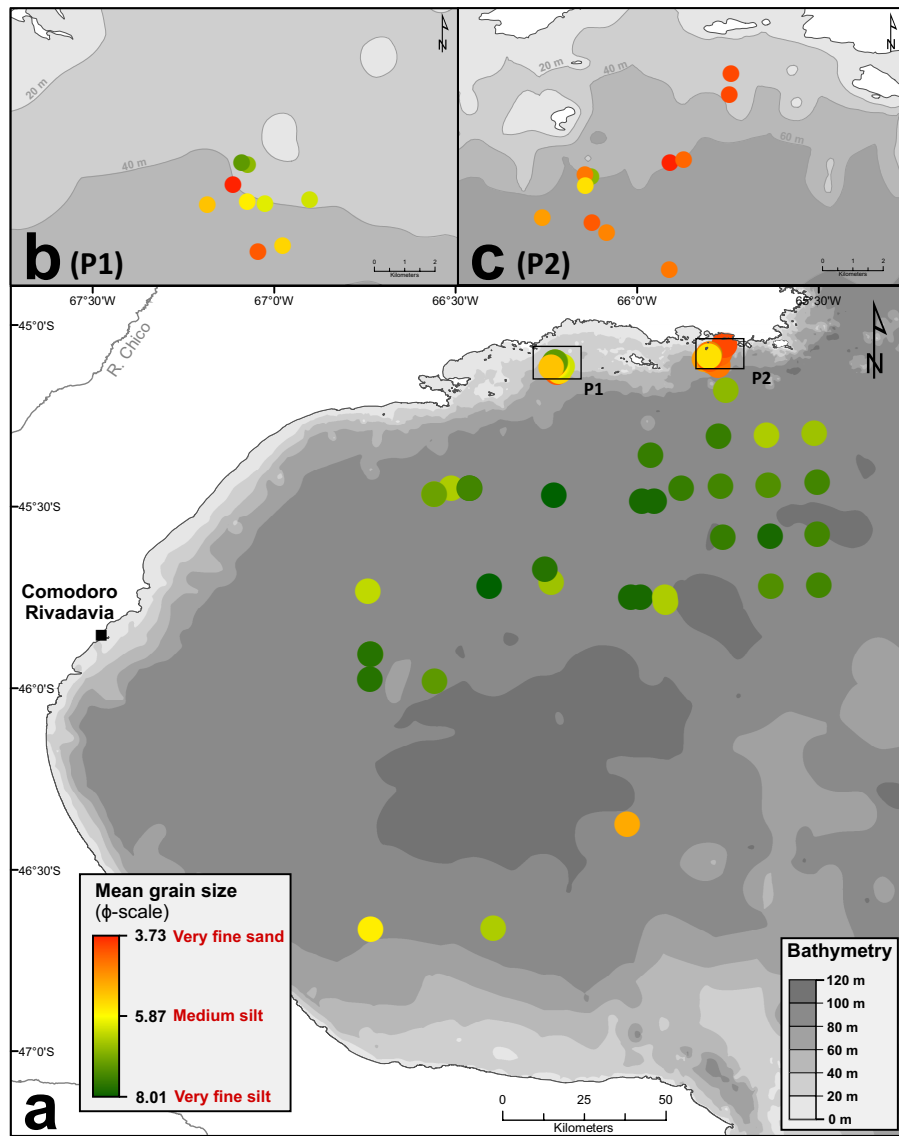


FIGURE S1. Spatial distribution of the mean grain-size for the surface sediments in (a) the Gulf of San Jorge (GSJ) and (b and c) marine park areas.

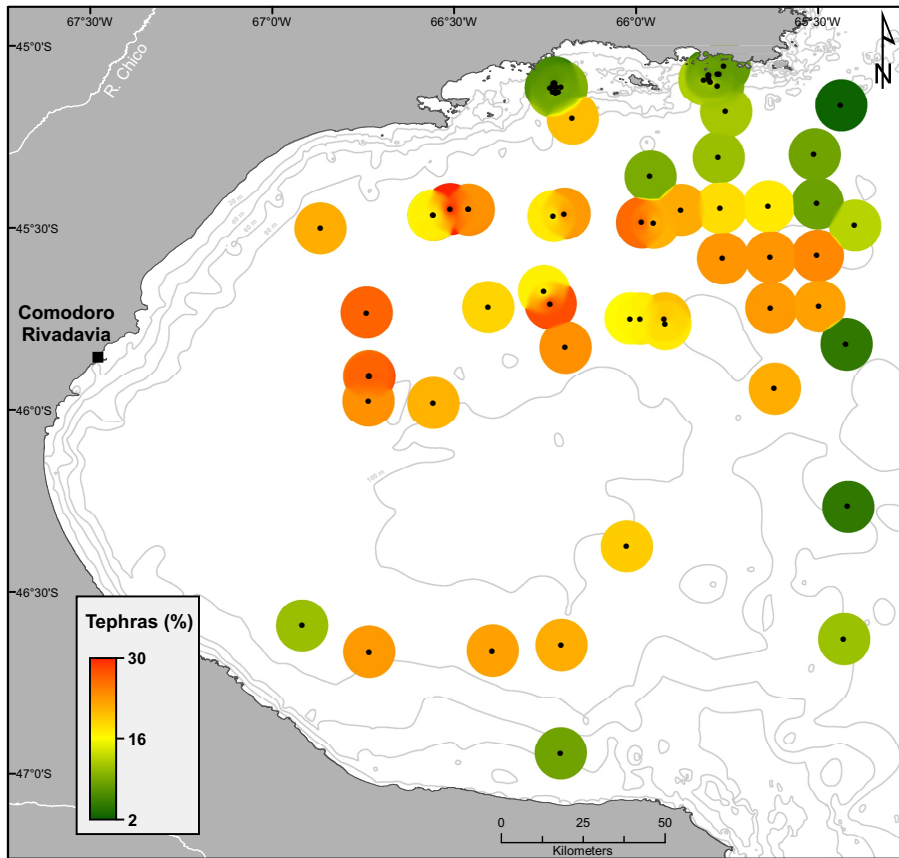


FIGURE S2. Spatial distribution of tephra (i.e., volcanic rhyolitic tephra) concentrations in the GSJ.

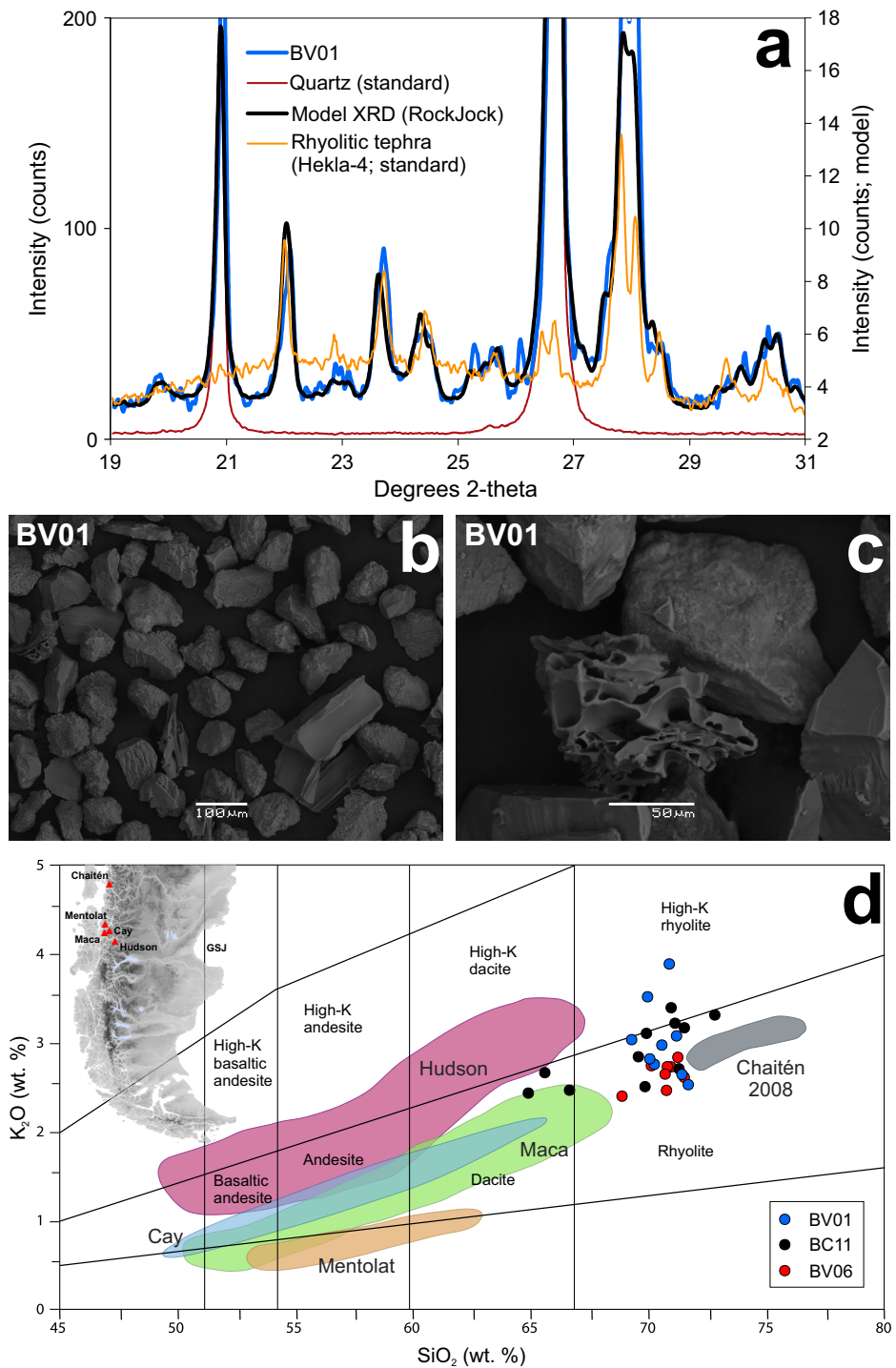


FIGURE S3. (a) Comparison of measured X-ray diffractogram and calculated best-fit curve obtained from RockJock v11 on a representative sample (BV01). The quartz and rhyolitic tephra (Hekla-4) standard used in the XRD analysis are also shown for comparison. (b–c) Scanning electron microscopy (SEM) images of the 300–63 μm fraction of surface sediment sample BV01. (d) K_2O vs. SiO_2 classification diagram for glass shards from BV01, BV06, and BC11 surface samples. The geochemical composition field of different volcanic provinces of the southern part of the SVZ (Carel et al., 2011, and references therein) and ashes from the 2008 Chaitén eruption (Watt et al., 2009; Ruggieri et al., 2012) are presented for comparison.

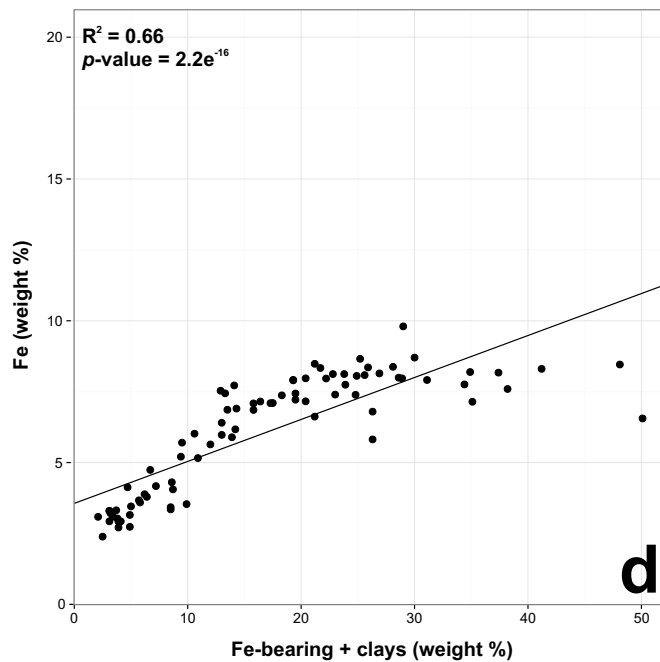
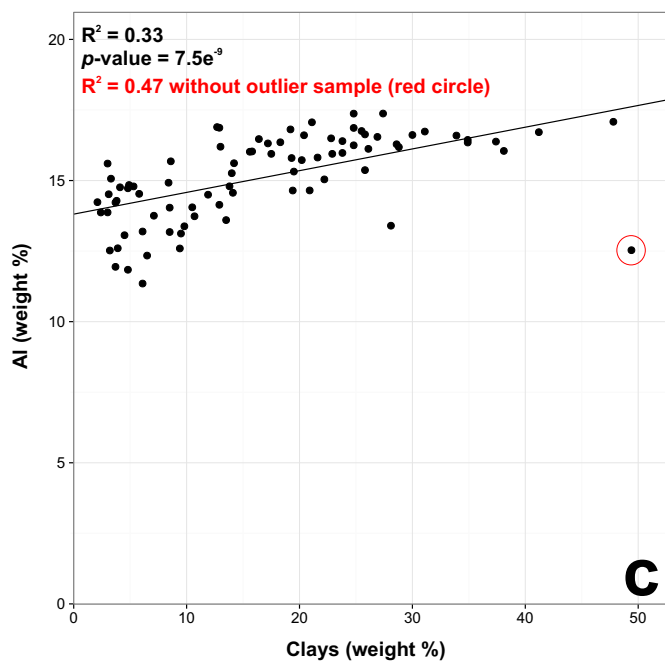
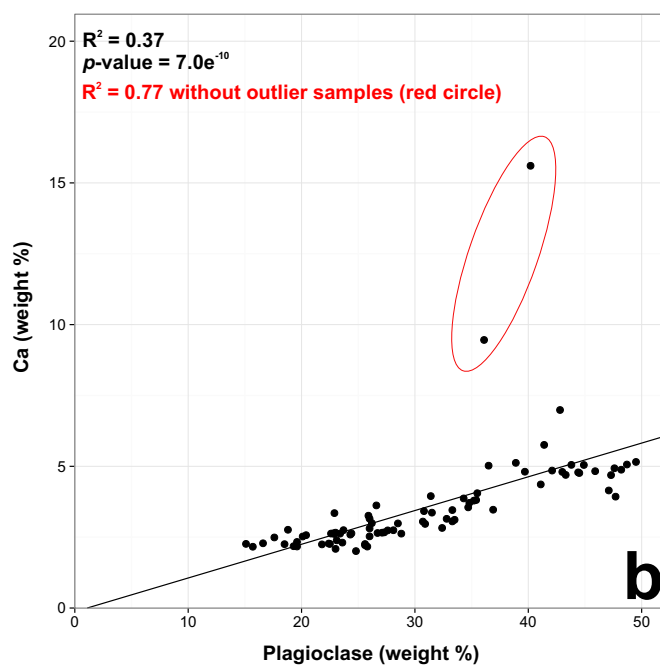
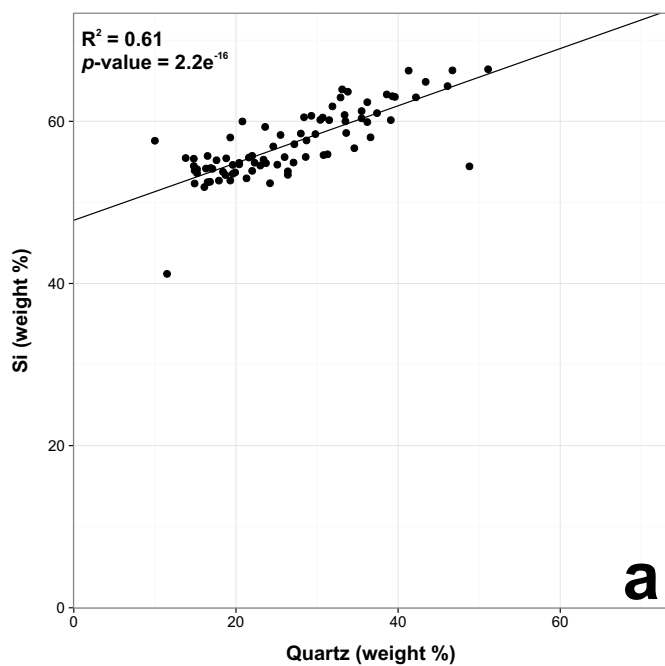


FIGURE S4. (a) Weight % Si plotted vs. weight % quartz. (b) Weight % Ca plotted vs. weight % plagioclase. (c) Weight % Al plotted vs. weight % clays. (d) Weight % Fe plotted vs. weight % Fe-bearing + chlorite + clays.

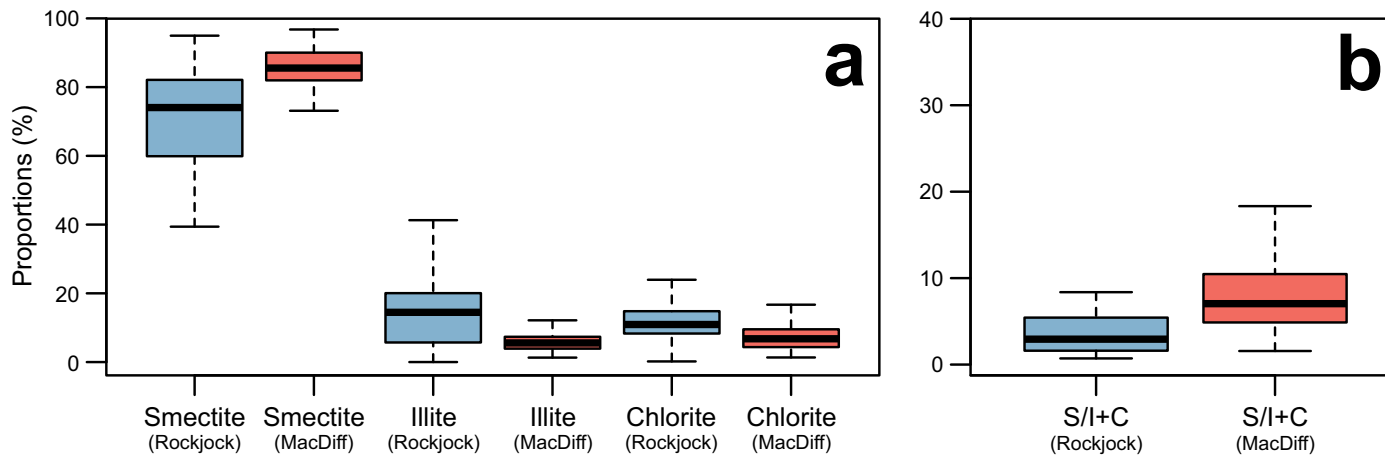


FIGURE S5. (a) Box plot illustrating the smectite (S), illite (I), and chlorite (C) relative concentrations of GSJ sediment samples as yielded by RockJock and oriented mounted methods (<2 μm ; MacDiff). (b) Box plot of ratios S/I+C and S/I+C showing the relative clays compositions of GSJ sediment samples as yielded by RockJock and oriented mounted methods (<2 μm).

FIGURE S1. Spatial distribution of the mean grain-size for the surface sediments in (a) the Gulf of San Jorge (GSJ) and (b and c) marine park areas.

FIGURE S2. Spatial distribution of tephra (i.e., volcanic rhyolitic tephra) concentrations in the GSJ.

FIGURE S3. (a) Comparison of measured X-ray diffractogram and calculated best-fit curve obtained from RockJock v11 on a representative sample (BV01). The quartz and rhyolitic tephra (Hekla-4) standard used in the XRD analysis are also shown for comparison. (b–c) Scanning electron microscopy (SEM) images of the 300–63 μm fraction of surface sediment sample BV01. (d) K_2O vs. SiO_2 classification diagram for glass shards from BV01, BV06, and BC11 surface samples. The geochemical composition field of different volcanic provinces of the southern part of the SVZ (Carel et al., 2011, and references therein) and ashes from the 2008 Chaitén eruption (Watt et al., 2009; Ruggieri et al., 2012) are presented for comparison.

FIGURE S4. (a) Weight % Si plotted vs. weight % quartz. (b) Weight % Ca plotted vs. weight % plagioclase. (c) Weight % Al plotted vs. weight % clays. (d) Weight % Fe plotted vs. weight % Fe-bearing + chlorite + clays.

FIGURE S5. (a) Box plot illustrating the smectite (S), illite (I), and chlorite (C) relative concentrations of GSJ sediment samples as yielded by RockJock and oriented mounted methods (<2 μm ; MacDiff). (b) Box plot of ratios S+I/C and S/I+C showing the relative clays compositions of GSJ sediment samples as yielded by RockJock and oriented mounted methods (<2 μm).

TABLE S1. Mean grain size and End-member (EM) scores for surface sediments of the Gulf of San Jorge (GSJ).

TABLE S2. Mineral composition of bulk and clay fraction of sediment samples.

TABLE S3. Chemical composition of sediment samples.

TABLE S4. Sources contributing to surface samples.

TABLE S5. (a) Minerals identified in RockJock v11, (b) consolidated list of minerals, (c) minerals used in SedUnMix, and (d) samples associated to sources in SedUnMix.